

**Decentralised Velocity Feedback Control Unit using a
Triangular Piezoelectric Actuator**

D. Emo and P. Gardonio

ISVR Technical Memorandum No 950

August 2005



SCIENTIFIC PUBLICATIONS BY THE ISVR

Technical Reports are published to promote timely dissemination of research results by ISVR personnel. This medium permits more detailed presentation than is usually acceptable for scientific journals. Responsibility for both the content and any opinions expressed rests entirely with the author(s).

Technical Memoranda are produced to enable the early or preliminary release of information by ISVR personnel where such release is deemed to be appropriate. Information contained in these memoranda may be incomplete, or form part of a continuing programme; this should be borne in mind when using or quoting from these documents.

Contract Reports are produced to record the results of scientific work carried out for sponsors, under contract. The ISVR treats these reports as confidential to sponsors and does not make them available for general circulation. Individual sponsors may, however, authorize subsequent release of the material.

COPYRIGHT NOTICE

(c) ISVR University of Southampton All rights reserved.

ISVR authorises you to view and download the Materials at this Web site ("Site") only for your personal, non-commercial use. This authorization is not a transfer of title in the Materials and copies of the Materials and is subject to the following restrictions: 1) you must retain, on all copies of the Materials downloaded, all copyright and other proprietary notices contained in the Materials; 2) you may not modify the Materials in any way or reproduce or publicly display, perform, or distribute or otherwise use them for any public or commercial purpose; and 3) you must not transfer the Materials to any other person unless you give them notice of, and they agree to accept, the obligations arising under these terms and conditions of use. You agree to abide by all additional restrictions displayed on the Site as it may be updated from time to time. This Site, including all Materials, is protected by worldwide copyright laws and treaty provisions. You agree to comply with all copyright laws worldwide in your use of this Site and to prevent any unauthorised copying of the Materials.

UNIVERSITY OF SOUTHAMPTON
INSTITUTE OF SOUND AND VIBRATION RESEARCH
SIGNAL PROCESSING AND CONTROL GROUP

**Decentralised Velocity Feedback Control Unit using a Triangular
Piezoelectric Actuator**

by

D. Emo and P. Gardonio

ISVR Technical Memorandum N°950

August 2005

Authorized for issue by
Professor S.J. Elliott
Group Chairman

ABSTRACT

In this report, the stability of a new type of Direct Velocity Feedback control loop using triangular piezoelectric actuators bonded on smart panels has been studied. Direct Velocity Feedback control systems allow a good reduction of the transmitted sound pressure level. However, their performance is limited by their stability at high frequencies. A previous theoretical work has shown that the triangularly shaped actuators are more efficient than square actuators, but the stability of these actuators has not been studied in details yet. In this work, the parameters of the triangles have been studied so as to find the optimal set up, which allows a high performance and stability. In particular, the height, the base and the size of the triangular patches have big effects on the stability, since they have a big influence on the actuator's transfer function. This study shows it is possible to find an optimal set of parameters, which allows obtaining an efficient and stable system. The effects of the accelerometers on the system's stability have also been analysed, so that it is possible to design an optimal feedback loop.

TABLE OF CONTENTS

ABSTRACT.....	3
TABLE OF CONTENTS	4
TABLE OF FIGURES.....	6
INTRODUCTION	9
1. SMART PANEL USING 16 TRIANGULAR PIEZOELECTRIC ACTUATORS	10
1.1. DIRECT VELOCITY FEEDBACK CONTROL.....	10
1.2. SMART PANEL WITH 16 TRIANGULAR ACTUATORS.....	13
1.2.1. <i>Response and sound transmission of the panel without active control</i>	13
a) Analytical model	13
b) Response of the panel.....	15
1.2.2. <i>Response and sound transmission of the panel with active control</i>	16
a) The active control system.....	16
b) Analytical model with active control.....	18
c) Theoretical performance of the system with 16 actuators	20
2. SINGLE LOOP STABILITY.....	23
2.1. REVIEW ON STABILITY – NYQUIST CRITERION.....	23
2.2. OPEN LOOP RESPONSE FUNCTION.....	25
2.3. PARAMETRICAL STUDY.....	31
2.3.1. <i>Influence of the actuator's height</i>	32
2.3.2. <i>Influence of the actuator's base length</i>	37
2.3.3. <i>Influence of the size of the actuator</i>	39
2.3.4. <i>Optimal set of parameters</i>	40
2.4. INFLUENCE OF THE ACCELEROMETERS	42
2.4.1. <i>Analytical model with accelerometer</i>	42
2.4.2. <i>Effect on the frequency response function</i>	45
2.4.3. <i>Influence of the position of the accelerometers</i>	48
3. CLOSED LOOP SYSTEM'S EFFICIENCY	52
3.1. FREQUENCY RESPONSE FUNCTION OF THE WHOLE FEEDBACK LOOP	52
3.2. RESPONSE AT THE CONTROL POINT WITH VELOCITY FEEDBACK CONTROL.....	53
4. PERSPECTIVES.....	56
5. CONCLUSION.....	57
ACKNOWLEDGEMENTS	59

REFERENCES61
ANNEXES63

TABLE OF FIGURES

Figure 1: <i>scheme of a 1 dof isolation system: a) with passive damper; b) with both passive and active dampers; c) with a passive damper and an equivalent skyhook passive damper to the active damper.</i>	10
Figure 2: <i>transmissibility of the systems shown on figure 1 with different damping ratios.</i>	11
Figure 3: <i>scheme of the panel without active control system.</i>	13
Figure 4: <i>panel's kinetic energy (left) and radiated power (right).</i>	15
Figure 5: <i>panel with the 16 triangular piezoelectric actuators.</i>	17
Figure 6: <i>stresses generated by a triangular piezoelectric patch.</i>	17
Figure 7: <i>scheme of the closed loop system.</i>	20
Figure 8: <i>total kinetic energy (a) and sound transmission ratio (b) of the panel with feedback gains of 0 (solid line), 10 (faint line), 100 (dash-dotted line), 1000 (dotted line) and 10000 (bold line).</i>	21
Figure 9: <i>normalized kinetic energy (a) and sound transmission ratio (b) integrated between 0 and 1 kHz.</i>	22
Figure 10: <i>classical bloc diagram of a closed loop system.</i>	23
Figure 11: <i>Nyquist plots of the closed loop transfer function of different types of a stable system (dashed line), a conditionally stable system (solid line) and an unstable system (dotted line). The red circle represents the Nyquist point.</i>	24
Figure 12: <i>Bode diagram (a) and Nyquist plot (b) of the simulated frequency response function of the actuator bonded on a simply supported panel; Bode diagram (c) and Nyquist plot (d) of the simulated frequency response function of the actuator bonded on a clamped panel; Bode diagram (e) and Nyquist plot (b) of the measured frequency response function of the actuator.</i>	26
Figure 13: <i>response of the actuator when only the point force (a), the moments on the base edge (b), the moments on the right edge (c) and the moments on the left edge (d) are considered. The predicted phase lag is plotted with dash- dotted line.</i>	29
Figure 14: <i>parameters used to assess performance and stability of a system.</i>	32
Figure 15: <i>variation of the δ ratio with the height of the actuator.</i>	33
Figure 16: <i>Bode diagrams and Nyquist plots with a height of 10 mm (1st row), 27 mm (2nd row) and 47 mm (3rd row) – simulated responses.</i>	34
Figure 17: <i>Bode diagram of the response due to only the moments on the left edge of the triangle with a height of 10 mm.</i>	35
Figure 18: <i>frequencies of the three first drops as a function of the height of the actuator.</i>	35

Figure 19: <i>Bode diagram and Nyquist plot of the measured response with a height of 10 mm</i>	36
Figure 20: <i>variation of the δ ratio with the base length of the actuator</i>	37
Figure 21: <i>Bode diagram and Nyquist plot of the simulated response with a base of 20 mm</i>	38
Figure 22: <i>frequencies of the first drops as a function of the base length of the actuator</i>	38
Figure 23: <i>variation of the δ ratio with the size of the actuator</i>	39
Figure 24: <i>frequencies of the three first drops as a function of the size of the actuator</i>	40
Figure 25: <i>variation of δ with the height and the base length of the triangular actuators</i>	41
Figure 26: <i>Bode diagram of the frequency response function of an accelerometer</i>	42
Figure 27: <i>scheme of an accelerometer mounted on the panel</i>	43
Figure 28: <i>Bode diagram and Nyquist plot of the response with an accelerometer</i>	46
Figure 29: <i>variation of the δ criterion with the resonance frequency of the accelerometer</i>	46
Figure 30: <i>Bode diagrams and Nyquist plots of the simulated and measured responses with accelerometer</i>	48
Figure 31: <i>scheme showing the different positions of the accelerometer</i>	49
Figure 32: <i>measured responses at the 3 positions (left: Bode, right: Nyquist)</i>	50
Figure 33: <i>scheme of the closed loop system</i>	52
Figure 34: <i>frequency response function of the feedback loop with optimized feedback gain</i>	53
Figure 35: <i>measured velocity at the control point with active velocity feedback control for different frequency ranges. Results with one control unit</i>	54

INTRODUCTION

Passive sound radiation control treatments have proven to be efficient in the high frequency range. However, they have no effect in the low frequency range, where the response of the radiating structure is characterised by well-separated resonances. That is the reason why Active Structural Acoustic Control (ASAC) systems have been developed.

In the following study, the response of a flat baffled smart panel associated with sixteen decentralised direct velocity feedback control systems is analysed. Each control system consists of a triangularly shaped piezoelectric actuator, whose base edge is aligned along the border of the panel, and a velocity sensor mounted at its tip. The signal given by the velocity sensor is fed back into the actuator, which generates a transverse force at its tip. As this force is proportional to velocity, it can be regarded as a damping force. Thus the sixteen independent control units generate a damping effect that tends to reduce the response of the panel in correspondence to the well-separated low frequency resonances.

The study presented in this report is focussed on the stability of one control unit. This is a key study to establish whether stable and robust control loops can be designed and thus whether relatively large control gains can be implemented. High feedback gains will indeed generate a high damping effect, which reduces efficiently the response of the panel at low resonance frequencies.

In the first part of this work, the general concepts of Direct Velocity Feedback Control and active damping are briefly reviewed through the example of a single degree of freedom vibration control problem. The theoretical performance of the sixteen triangular piezoelectric actuators mounted on the vibrating panel is evaluated.

In the second part, the open loop response of one control unit bonded on the panel is analysed in order to study its stability, with ideal sensor and real accelerometers. The different geometrical parameters of the triangular actuators are considered in a parametrical study, which gives the best compromise in order to design the most efficient control loop. This analysis is completed by experiments.

In the last part, the efficiency of one closed loop is evaluated when the smart panel is excited by a point force.

1. SMART PANEL USING 16 TRIANGULAR PIEZOELECTRIC ACTUATORS

In this part, the theoretical performance of an active velocity feedback control system using 16 triangular actuators bonded on a simply supported and baffled panel has been studied. The instability phenomenon has not been taken into account.

1.1. Direct velocity feedback control

The concept of active damping is introduced by analysing the example of a single degree of freedom (dof) system consisting of an inertial mass associated to an elastic mount, which is excited by a vibrating base.

As shown on figure 1a, a simple damper associated to the spring can isolate the seismic mass from the vibrating base. This passive isolation system is able to reduce vibrations at relatively high frequencies but, as shown in figure 2, it also produces a fundamental resonance effect where large vibration transmission occurs.

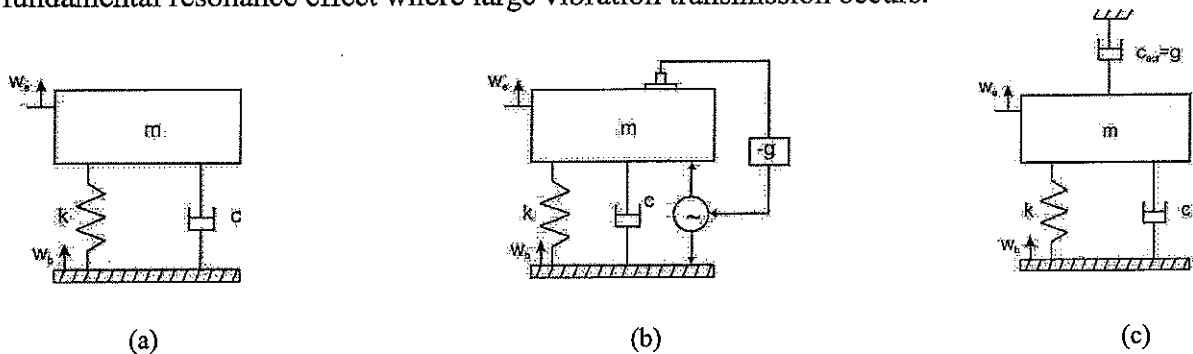


Figure 1: scheme of a 1 dof isolation system: a) with passive damper; b) with both passive and active dampers; c) with a passive damper and an equivalent skyhook passive damper to the active damper.

Indeed, to obtain a good isolation at this fundamental resonance frequency of the mass-spring system, it is necessary to have a high damping coefficient, which leads to a bad isolation at high frequencies. Active control can be used to improve the performances of the passive system. The system presented in the following study is a Direct Velocity Feedback control system: the sensor represented on figure 1b produces a signal proportional to the measured velocity of the seismic mass, which is fed back through a control gain into the vibrating system. Such a system is equivalent to a skyhook passive damper, as shown on figure 1c: it can be tuned so as to get a very good isolation at the resonance frequency of the

mass-spring system, while the passive damper can provide a good isolation at higher frequencies.

The transmissibility T of the single dof system is given by the following formula [3],

$$T(\Omega) = \frac{W_e(\Omega)}{W_b(\Omega)} = \frac{1 + 2j\xi_{pass}\Omega}{1 - \Omega^2 + 2j(\xi_{pass} + \xi_{act})\Omega} \quad (1)$$

where $\Omega = \frac{\omega}{\sqrt{km}}$ is the normalized frequency, $\xi_{pass} = \frac{c}{2\sqrt{km}}$ is the passive damping, w_e (respectively w_b) is the displacement of the seismic mass (respectively the displacement of the base), and $\xi_{act} = \frac{g}{2\sqrt{km}}$ is the active damping due to the feedback gain. This formula clearly shows that the active force acts like a damping force, since it is proportional to the velocity.

The transmissibility has been plotted (figure 2) for the passive isolation system with a small damping ratio ($\zeta_{pass}=0.1$), with a high damping ratio ($\zeta_{pass}=0.7$) and for the passive system enhanced with the feedback control ($\zeta_{pass}=0.1$ and $\zeta_{act}=0.6$).

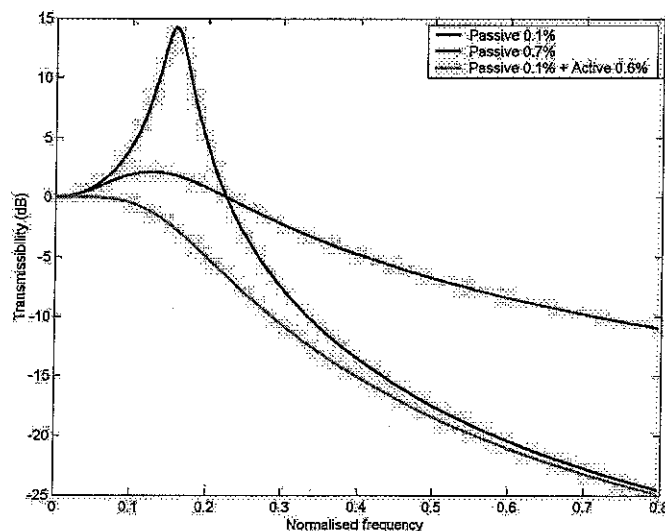


Figure 2: transmissibility of the systems shown on figure 1 with different damping ratios.

A high passive damping strongly reduces the amplitude at the resonance, but it also degrades the response at high frequencies, whereas the active control system is efficient over the whole frequency range.

An active control system can be characterised by three aspects:

- The performance
- The stability
- The robustness

The performance is the ability of the system to reduce efficiently the unwanted disturbances. Generally, an active control system is efficient in a relatively low frequency range.

The stability is a key point since it imposes the maximum feedback gain (and, as a consequence the maximum efficiency of the system) that can be used in the control loop. Two physical conditions have to be verified in order to have an unconditionally stable system: the duality and the collocation. The duality is the fact that the actuator and the sensor excite and detect the vibrations in the “same manner”, so that the product of the sensed response and the excitation is proportional to the power supplied to the system. The collocation is the fact that the sensor and the actuator are positioned at the same point. As those two conditions cannot obviously be respected in the reality, the control system can potentially go unstable [1].

The robustness is the ability of the system to remain efficient and stable even with small modifications of some parameters.

In the next part, the theoretical performance of the control system is studied with reference to the problem of active structural control of a panel excited with an acoustic plane wave.

1.2. Smart panel with 16 triangular actuators

1.2.1. Response and sound transmission of the panel without active control

The physical properties of the panel considered in this study are summarised in the following table:

Table 1: Physical properties of the panel.

Parameter	Value
Dimensions	$l_{xp} \times l_{yp} = 414 \times 314$ mm
Thickness	$h_p = 1$ mm
Mass density	$\rho_p = 2700$ kg/m ³
Young's modulus	$E_p = 7 \times 10^{10}$ N/m ²
Poisson ratio	$\nu_p = 0.33$
Modal damping ratio	$\zeta_n = 0.02$

The simulations have been carried out for a simply supported panel.

a) Analytical model

In the simulations, the simply supported panel is excited by a harmonic plane wave which is assumed to excite the panel with azimuthal and elevation angles of 45°, so that all structural modes are excited [2]. The panel is represented on the following scheme:

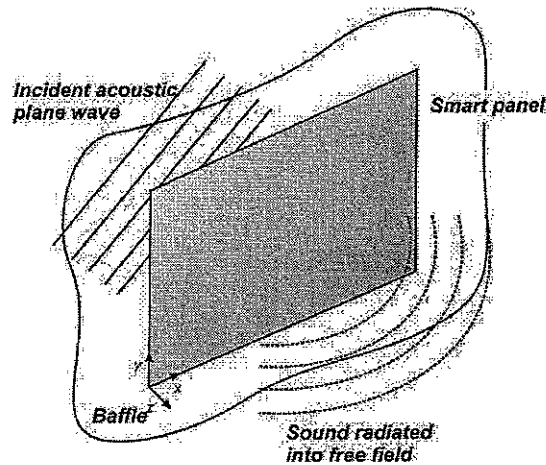


Figure 3: scheme of the panel without active control system.

An analytical model has been developed, which allows computations up to relatively high frequencies. The Euler – Bernoulli theory has been used, which means that only the bending waves are considered. As the shearing effect only occurs at very high frequencies (around 1 MHz for this panel), this assumption is acceptable for this study.

The panel is divided into a grid of R square elements. The phasors of the complex transverse velocities at the centers of these elements have been grouped into the following column vector:

$$\mathbf{w}_e(\omega) = \begin{Bmatrix} \dot{w}_{e1}(\omega) \\ \vdots \\ \dot{w}_{eR}(\omega) \end{Bmatrix} \quad (2)$$

The structural vibration of the panel is given by the acoustic primary excitation generated by the incident plane wave. Thus, the velocity column vector is given by [2]:

$$\mathbf{w}_e(\omega) = \mathbf{Y}_{ep}(\omega) \cdot p_i(\omega) \quad (3)$$

The elements in the mobility matrix of Eq. (3) have been calculated with a finite modal expansion, so that

$$\mathbf{Y}_{ep}^{r,1}(\omega) = j\omega \sum_{n=1}^N \frac{\psi_n(x_r, y_r) \cdot F_{np}(\omega)}{\rho_p h_p l_{xp} l_{yp} (\omega_n^2 - \omega^2 + 2j\zeta_n \omega \omega_n)} \quad (4)$$

where ζ_n is the damping ratio, taken to be 0.02 in the simulations, N the number of modes taken into account in the simulation, ω_n and Ψ_n are respectively the n-th natural frequency and natural mode of the panel (see annexe).

F_{np} is the modal excitation term due to the acoustic excitation. It is obtained by integrating the pressure field generated over the panel surface [2]:

$$F_{np}(\omega) = p_i(\omega) \cdot \int_0^{l_{xp}} \int_0^{l_{yp}} \psi_n(x, y) \cdot e^{-j(k_x x + k_y y)} dx dy = 4 \cdot p_i(\omega) \cdot I_m \cdot I_n \cdot l_{xp} \cdot l_{yp} \quad (5)$$

I_m and I_n are two terms that take into account the coupling between the acoustic plane wave and the vibrating panel.

Knowing the velocity of each element, it is possible to evaluate the kinetic energy and the sound power radiation [2].

$$E(\omega) = \frac{M_e}{4} \cdot \mathbf{w}_e^H \cdot \mathbf{w}_e \quad (6)$$

$$W_r(\omega) = \mathbf{w}_e^H \cdot \mathbf{R} \cdot \mathbf{w}_e \quad (7)$$

where M_e is the mass of each square element, R the radiation matrix of the panel (see annexe), and H the Hermitian transpose.

b) Response of the panel

The kinetic energy and the radiated sound power of the panel have been calculated in the frequency range 20 Hz – 50 kHz.

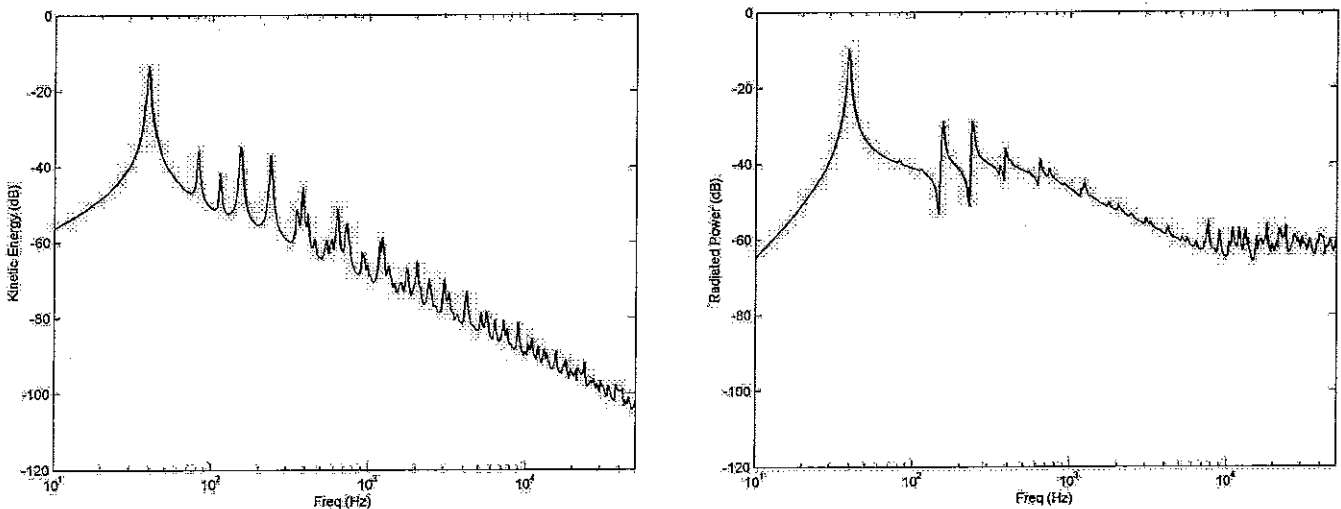


Figure 4: panel's kinetic energy (left) and radiated power (right).

Up to 3 kHz, the dynamical behaviour of the panel is characterised by well-separated resonances, some of which are also responsible for the transmitted sound. In this frequency range, there is almost no modal overlap, so that the panel's behaviour is only controlled by the resonant modes. Some of the modes don't have good radiation efficiency, and don't transmit much sound. This is the case for the 2nd and the 3rd mode (about 800 and 1000 Hz).

Beyond this frequency range, the dynamics of the panel is due to the contribution of many modes that are overlapping. This is the reason why it becomes impossible to distinguish the resonances at higher order modes in the radiated power. In this frequency range, the radiated sound power is controlled by the mass of the panel.

From about 10 kHz, the radiated power is maintained at the same level whereas the kinetic energy keeps going down, because there is coincidence between the wavelengths in the air and in the material. (the coincidence frequency of the plate is equal to 12.9 kHz).

The behaviour below 3 kHz is interesting since the radiated power is only due to the resonant modes. By controlling these resonant modes, it is possible to reduce the transmitted power. Resonances can be efficiently controlled with damping, eg active damping, that's why the active velocity feedback control described in part 1.1 has been used to reduce the radiated power.

1.2.2. Response and sound transmission of the panel with active control

a) The active control system

As shown in figure 5, the control system considered in this study is made of 16 triangular piezoelectric actuators evenly distributed along the panel's edges [2]. As explained in part 1.1, each control unit acts like a skyhook damper, so that this system tends to create anechoic boundary conditions that prevent the creation of reflecting waves and as a consequence of modes.

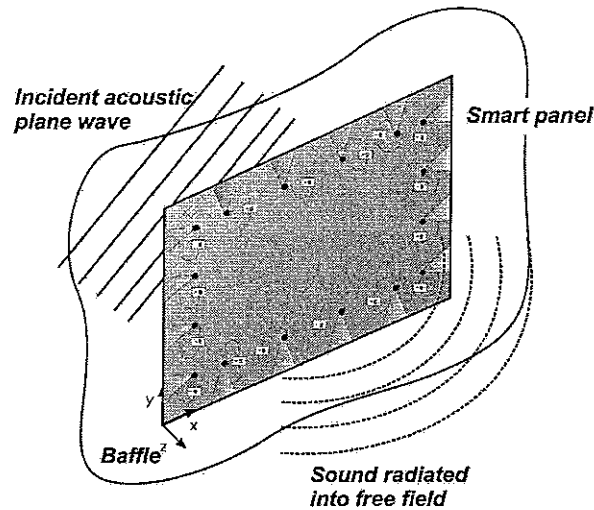


Figure 5: *panel with the 16 triangular piezoelectric actuators.*

When a voltage is applied to the piezoelectric patches, strains are created on the three edges of the triangles, and thus, because the patch is mounted off the middle plane of the panel, moments are created along the edges. Also, as shown in figure 6, point forces are generated at the three vertices [4].

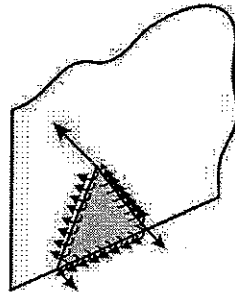


Figure 6: *stresses generated by a triangular piezoelectric patch.*

As the triangular piezoelectric actuators are placed on the edges of the simply supported panel, the two forces on the base are compensated by the reaction of the frame, and have no effect on the behaviour of the vibrating panel. Thus, they have been taken equal to zero in the theoretical study.

The triangular actuators are made of a piezoelectric PZT ceramic, which are well adapted to active control, since they are able to produce relatively strong stresses when

bonded to a system. The properties of this ceramic material are summarised in the following table:

Table 2: *physical properties of the piezoelectric material*

Parameter	Value
Material	Pz27
Base and height	$b \times a = 40 \times 25$ mm
Thickness	$h_{PZT} = 0.5$ mm
Density	$\rho_{PZT} = 7600$ kg/m ³
Young's modulus	$E_{PZT} = 6.3 \times 10^{10}$ N/m ²
Poisson ratio	$\nu_{PZT} = 0.29$
PZT strain/charge constants	$d_{31}^0 = 166 \times 10^{-12}$ m/V
	$d_{32}^0 = 166 \times 10^{-12}$ m/V
	$d_{36}^0 = 0$ m/V

The sensors are accelerometers placed at the top of the triangles. Because of the two forces on the base and the moments, duality and collocation are not respected. However, the force that is produced at the top of the triangle has high amplitude in comparison to the other forces, which improves the collocation. That is the reason why the triangular shape is supposed to give a better performance to the control system. The measured response is integrated to get a signal which is proportional to the velocity, and then fed back into the system.

b) Analytical model with active control

In this part, the sensors are still considered as ideal velocity sensors and the effect of the accelerometers is not taken into account.

Using the formulation developed in part 1.2.1.a, it is possible to express the contribution of the piezoelectric actuators on the velocity of an element:

$$\mathbf{w}_e(\omega) = \mathbf{Y}_{ec}(\omega) \cdot \mathbf{v}_c(\omega) \quad (8)$$

where \mathbf{v}_c is a vector with the phasors of the complex input voltage to the S piezoelectric transducers.

The elements in the matrix of Eq. (8) have been calculated in the same manner as in Eq (4):

$$\mathbf{Y}_{ec}^{r,s}(\omega) = j\omega \sum_{n=1}^N \frac{\psi_n(x_r, y_r) \cdot F_{ns}(\omega)}{\rho_p h_p l_{xp} l_{yp} (\omega_n^2 - \omega^2 + 2j\zeta_n \omega \omega_n)} \quad (9)$$

F_{ns} is the modal excitation term due to the flexural excitations. This term is given by the following equation [2]:

$$F_{ns} = \frac{h_s}{2} (m^2 e_{31}^0 + e_{32}^0) \left\{ \int_{vs1}^{vs3} \frac{\partial \psi_n(x, y)}{\partial \mathbf{n}_{ls1}} dl_{s1} + \int_{vs2}^{vs3} \frac{\partial \psi_n(x, y)}{\partial \mathbf{n}_{ls2}} dl_{s2} \right\} \\ + \frac{h_s}{2} e_{31}^0 \int_{vs1}^{vs2} \frac{\partial \psi_n(x, y)}{\partial \mathbf{n}_{bs}} db_s + 4 \frac{h_s}{2} m e_{31}^0 \psi_n(x_{vs3}, y_{vs3}) \quad (10)$$

where $vs_i=(x_i, y_i)$ are the coordinates of the three tops of the triangle.

Then, assuming the system is linear, the total velocity vector is given by:

$$\mathbf{w}_e(\omega) = \mathbf{Y}_{ep}(\omega) \cdot p_i(\omega) + \mathbf{Y}_{ec}(\omega) \cdot \mathbf{v}_c(\omega) \quad (11)$$

In particular, the velocity at the control point is given by:

$$\dot{\mathbf{w}}_c(\omega) = \mathbf{Y}_{cp}(\omega) \cdot p_i(\omega) + \mathbf{Y}_{cc}(\omega) \cdot \mathbf{v}_c(\omega) \quad (12)$$

As shown on figure 7, $\dot{\mathbf{w}}_c(\omega)$ can be expressed in term of the acoustic pressure only. Thus:

$$\dot{\mathbf{w}}_c(\omega) = [\mathbf{I} + \mathbf{Y}_{cc}(\omega) \cdot \mathbf{H}(\omega)]^{-1} \cdot \mathbf{Y}_{cp}(\omega) \cdot p_i(\omega) \quad (13)$$

$$\mathbf{v}_c(\omega) = -\mathbf{H}(\omega) \cdot [\mathbf{I} + \mathbf{Y}_{cc}(\omega) \cdot \mathbf{H}(\omega)]^{-1} \cdot \mathbf{Y}_{cp}(\omega) \cdot p_i(\omega) \quad (14)$$

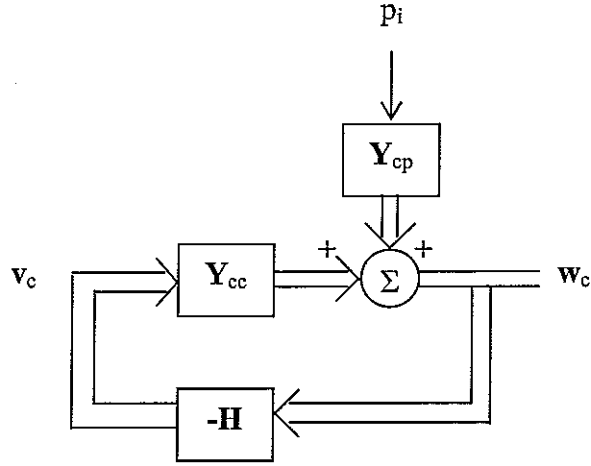


Figure 7: scheme of the closed loop system

Finally the phasors vector of the velocity at the centers of the elements of the panel can be expressed in term of only the acoustic excitation:

$$\dot{w}_e(\omega) = Y_{ep}(\omega) \cdot p_i(\omega) - Y_{ep}(\omega) \cdot H(\omega) \cdot [I + Y_{cc}(\omega) \cdot H(\omega)]^{-1} \cdot Y_{cp}(\omega) \cdot p_i(\omega) \quad (15)$$

The kinetic energy of the panel and the radiated sound power are then given by equations 6 and 7.

The actual system is a decentralised control system, which means that each control loop (eg each actuator) is working independently from the others. In other terms, the control force produced by a triangular actuator is only dependant on the signal measured at the top of this actuator. As a consequence, the H matrix is diagonal, and in order to simplify the controller, it is taken equal to $h \cdot I$, where I is the 16x16 identity matrix and h the feedback gain.

c) Theoretical performance of the system with 16 actuators

The kinetic energy and the radiated sound power have been plotted in the frequency range 0 – 1000 Hz for different feedback gains.

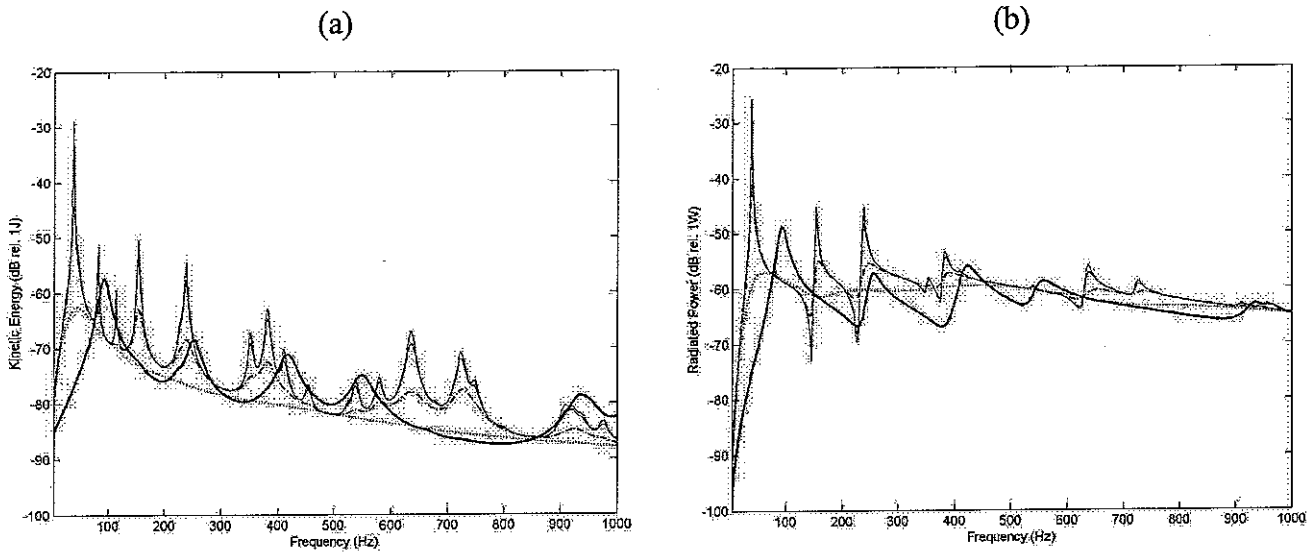


Figure 8: total kinetic energy (a) and sound transmission ratio (b) of the panel with feedback gains of 0 (solid line), 10 (faint line), 100 (dash-dotted line), 1000 (dotted line) and 10000 (bold line).

As expected, the kinetic energy is theoretically strongly reduced when the feedback gain increases. With higher feedback gains, the active damping becomes indeed stronger, which reduces the amplitude of the response at the resonance peaks. As the radiated power is mainly due to single resonant modes in this frequency range, reducing the amplitude of these modes also reduces the radiated sound power, which is confirmed by the results on figure 8b.

For very high feedback gains, new resonance peaks appear: when a very high feedback gain is used, the actuation becomes so strong that the vibrations at the control points are cancelled. The triangles act as if they were pinning the panel, which changes its dynamics. The panel is stiffened, and as a consequence the resonance frequencies are increased. In such a case, it is clear that the system is not as efficient as for smaller feedback gains, since the amplitude of the resonance peaks increases. This phenomenon is illustrated in figure 9, which shows it is possible to find an optimal feedback gain, which leads to a minimum kinetic energy and radiated sound power. Over this optimal gain, the dynamics of the system is modified, and the system becomes less efficient.

The reduction of sound transmitted through the panel with the optimal gain (-10 dB) is lower than the reduction that can be achieved with the kinetic energy (-18 dB). It is due to the fact that the active control is in that case a structural active control: the aim is to reduce the amplitude of the resonant modes, so that they don't radiate too much. As their radiation

efficiency is not always very high, controlling these modes doesn't necessarily mean reducing the transmitted sound power.

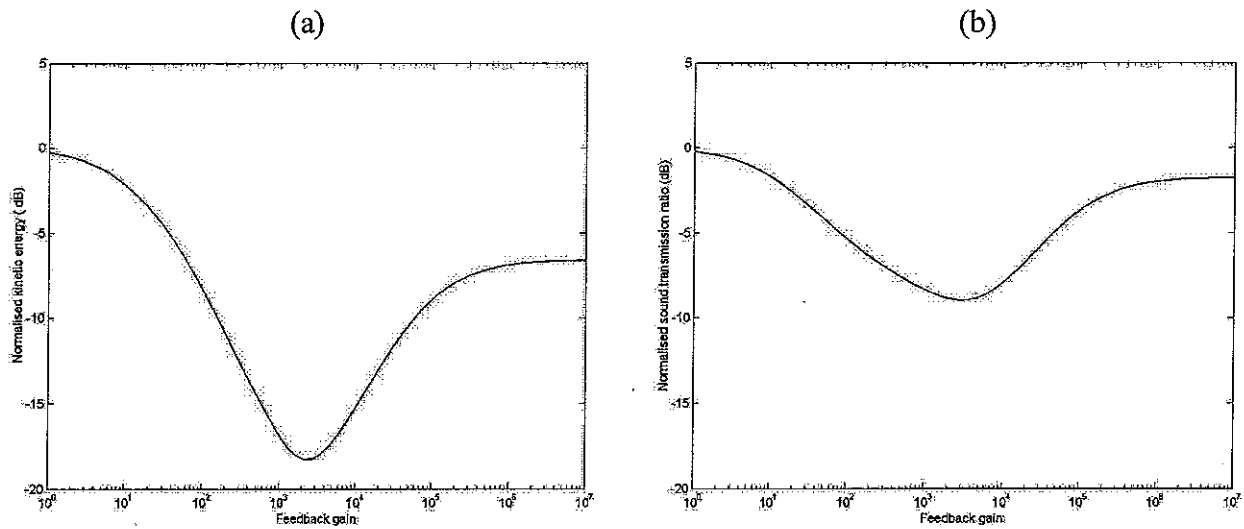


Figure 9: *normalized kinetic energy (a) and sound transmission ratio (b) integrated between 0 and 1 kHz*

However, because of instability problems, it is impossible to use the optimal feedback gain without risking damaging the system. This is the reason why it is necessary to design an actuator that gives a feedback loop as stable as possible, so that the optimal feedback gain can be implemented without instability problems.

2. SINGLE LOOP STABILITY

In this section, the stability of a single loop has been studied in order to design an optimal actuator. A parametrical study has been made to find the best set of parameters to obtain a stable system.

2.1. Review on stability – Nyquist criterion

The scheme in figure 10 represents the bloc diagram of a closed loop system.

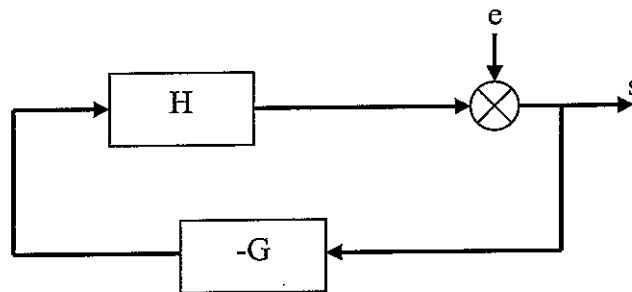


Figure 10: classical bloc diagram of a closed loop system

The transfer function of such a system is given by:

$$\frac{s}{e} = \frac{1}{1+GH} \quad (16)$$

where s is the output, e is the input, G is the feedback gain and H the plant response of the system.

As soon as $GH=-1$, the transfer function diverges, and the closed loop system becomes unstable. As a consequence, in order to study a closed loop system's stability, it is necessary to analyse the open loop, which is in this case equal to GH .

The usual criterion that is used to assess the stability of a closed loop system is the Nyquist criterion, which says that if the curve representing the open loop transfer function of this system in the Nyquist plot encloses the point $(-1, 0)$, the system is unstable. However, it is often necessary to distinguish several cases:

1. if the curve encloses the point $(-1, 0)$, the system is unstable.
2. if the curve remains in the right hand side of the Nyquist plot (eg the real part of the open loop transfer function is always positive), the system is unconditionally stable.
3. if a part of the curve belongs to the left hand side of the Nyquist plot (eg the real part of the open loop transfer function has negative values), the system is only conditionally stable. In that case, the system can go unstable if the gain of the feedback loop (G) is increased, because the size of the loops is proportional to the feedback gain. The relevant criterion to assess the stability of the system is then the gain margin, which is equal to $\frac{1}{\delta}$ (see figure 11). The bigger the gain margin is, the bigger the feedback gain can be, which means that the system can be more efficient.

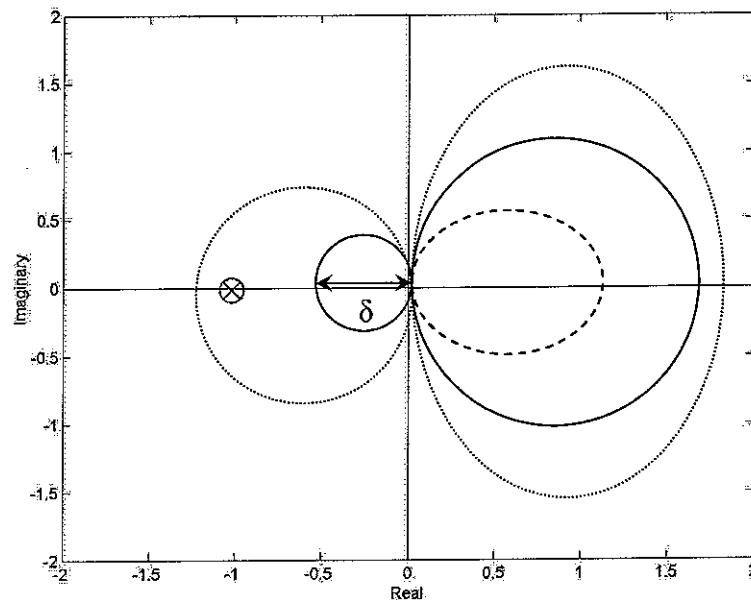


Figure 11: Nyquist plots of the closed loop transfer function of different types of a stable system (dashed line), a conditionally stable system (solid line) and an unstable system (dotted line). The red circle represents the Nyquist point.

In the case of the active control system using triangular actuators, the open loop transfer function is equal to (Eq 13): $Y_{cc}(\omega) \cdot H(\omega)$. In the following section, only $Y_{cc}(\omega)$ is studied.

2.2. Open loop response function

The reference dimensions of the actuators are those described in part 1.2.2.a. In this section, the sensors are considered ideal, which means that the signal they produce is directly proportional to the velocity measured at the top of the triangles. The measurements have been made with a laser vibrometer, which has no mechanical effect on the structure. Thus, only the characteristics of the actuator are taken into account in this study, so that their effect on the stability can be analysed independently from the effect of the other components of the feedback loop (accelerometer, integrator, amplifier). As it will be discussed in the following part, the boundary conditions can neither be considered as clamping boundary conditions, nor as simply supported boundary conditions. This is the reason why both the theoretical responses of the actuator bonded on a clamped panel and on a simply supported panel have been plotted.

Theoretical response

At low frequencies (in red in figure 12), the amplitude of the response of the triangular actuator is quite high, and its phase is situated in the range $[-90^\circ \ 90^\circ]$: this means that the actuation is relatively strong and that the system remains stable in this frequency range. It can be seen on the Nyquist plot, since the corresponding loops are all situated on the right hand side, and all have big amplitude.

The second asset of this type of actuator is that the amplitude at the frequencies where instability phenomenon could occur is quite low (left hand side loops of the Nyquist plot, which correspond to frequencies below 1kHz). Thus, the gain margin is quite important, so that it is possible to use high feedback gains, which will improve the efficiency of the system at low frequencies without making it be unstable. In fact, an accurate look on the response of the system shows that it is efficient over a relatively large frequency range, since the Nyquist plot of the open loop response function is mainly situated on the right hand side of the graph. According to both the Bode diagram and the Nyquist plot, instabilities can only occur at frequencies around 3500 Hz and 25 kHz, which correspond to the frequencies of the drop that can be seen on the amplitude. At these frequencies, the Nyquist plot of the open loop transfer function is situated on the left hand side of the graph, but, as the amplitude is quite low, it does not affect much the stability.

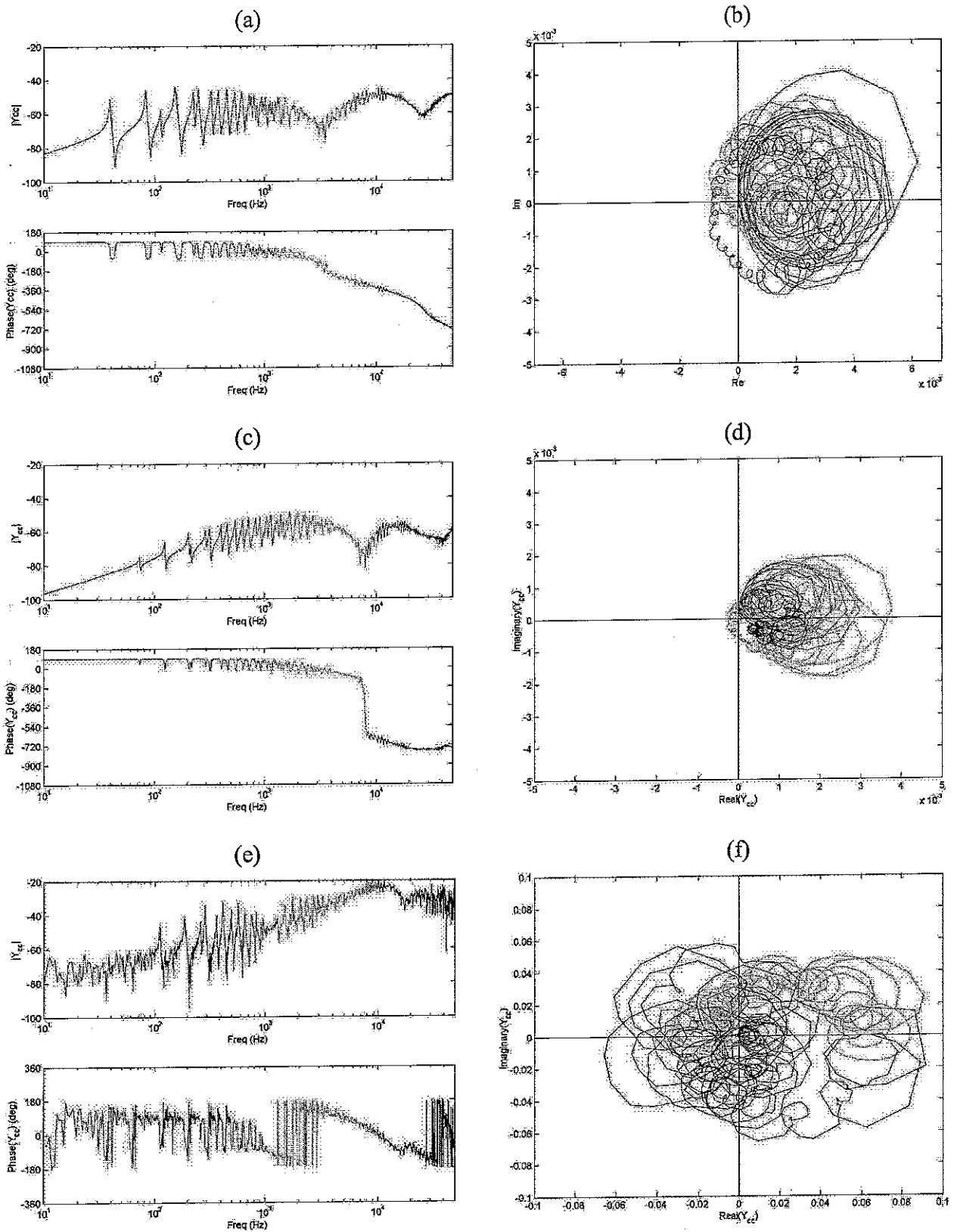


Figure 12: Bode diagram (a) and Nyquist plot (b) of the simulated frequency response function of the actuator bonded on a simply supported panel; Bode diagram (c) and Nyquist plot (d) of the simulated frequency response function of the actuator bonded on a clamped panel; Bode diagram (e) and Nyquist plot (b) of the measured frequency response function of the actuator

The drops in the amplitude are a particularity of the triangular shape. They are due to a cancellation effect of the different stresses produced by the actuator. Because these different stresses are not applied at the same location, their effect at the sensor's position is seen with a phase lag, which leads to interferences that can reduce the amplitude of the response. This phase lag can be easily evaluated, knowing that the velocity of flexural waves in the plate is given by:

$$c_b = \sqrt{2\pi f} \cdot \sqrt{\frac{E \cdot h^2}{12 \cdot (1 - \nu^2) \cdot \rho}} \quad (17)$$

where f is the frequency, E the Young Modulus, ν the Poisson's coefficient, ρ the density and h the thickness of the plate.

Since the bending wavelength is given by:

$$\lambda = \frac{c_b}{f} \quad (18)$$

then

$$\lambda = \frac{3.13}{\sqrt{f}} \quad (19)$$

Therefore the phase lag created by a distance of h is equal to:

$$\varphi = -\frac{2\pi \cdot h}{\lambda} = -\frac{2\pi \cdot h \cdot \sqrt{f}}{3.13} \quad (20)$$

The Bode diagrams of the frequency response function of each component of the actuation (point force at the top and moments along the three edges) have been plotted to analyse their effect on the global response (figure 13). This has been made only for the actuator bonded on the simply supported panel, since the conclusions are similar with the clamped panel. For the diagrams showing the response due to the moments only, the theoretical phase lag at the position of the sensor has also been plotted. For the moments on

the base edge, h has been taken equal to the height of the triangle, which is in this case equal to 25 mm, and for the moments on the two other edges, h has been taken equal to 32 mm, which is the length of these edges. These values of h are obviously a strong hypothesis, since the distance to the top vertice is different for each single moment. However, these values are relevant to explain the phase lag.

The phase of the response due to the point force is always in the range $[-90^\circ, 90^\circ]$. This force does not bring any instability since it is perfectly collocated with the sensor.

The amplitude of the response due to the moments produced along the base of the triangle keeps increasing, whereas the phase goes down at high frequencies (figure 13b). This phenomenon is very bad for the stability because it means that the amplitude at the frequencies where instability phenomenon can occur is relatively high. The phase begins at -90° (instead of $+90^\circ$) because the moments on the base are equivalent to small forces applied in the opposite direction from the direction of the top vertices point force. A good agreement is seen with the phase prediction, although differences appear, mainly due to the fact that the coupling with the plate has not been taken into account in equation 18. In particular, the phase shifts due to the resonant modes don't appear on the predicted response.

The phase of the response due to the moments on the two other edges also goes down at high frequencies, which is confirmed by the predicted phase (figures 13c and 13d). The big drops in the phase are due to numerical rounding effects in the simulation. The amplitude at high frequencies is much lower (-10 dB) than the amplitude of the response due to the moments on the base. These moments bring instability as well, although this effect is not as important as for the base moments.

The previous analysis clearly shows that the non collocation between the actuator's effects and the sensor is responsible for instability, since it causes phase lags that bring the open loop response to the instability domain.

The first drop in the amplitude of the global response is mainly due to the moments produced on the base edge. The drops that can be observed at higher frequencies are due to the combination of all the moments and forces. Though, in that case, moments on the right and left edges have a bigger influence than for the first drop, because their response at high

frequencies is made of many drops (see figure 13c below 10 kHz). These drops seem to play a big role in the creation of the drops of the global response at high frequencies.

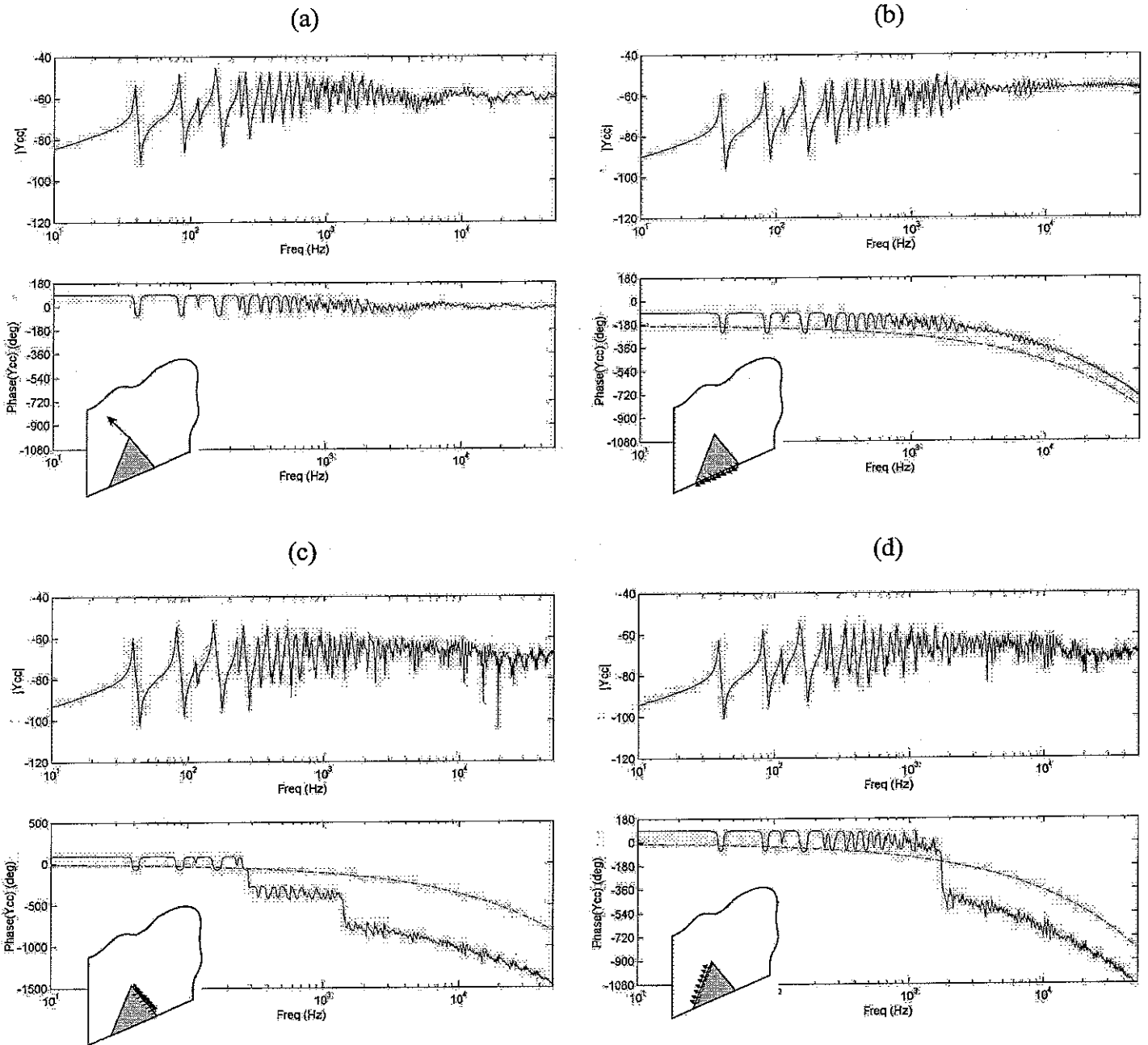


Figure 13: response of the actuator when only the point force (a), the moments on the base edge (b), the moments on the right edge (c) and the moments on the left edge (d) are considered. The predicted phase lag is plotted with dash- dotted line

Some differences obviously appear between the predicted response for the simply supported panel (figures 12a and 12b) and the predicted response for the clamped panel (figures 12c and 12d). In particular, the resonance frequencies are higher in the second case, which is logical since the panel is stiffer. This stiffening effect due to the clamping is also responsible for the fact that the amplitude goes up. However, the Nyquist plots are very similar in both cases, which is the most important criterion for the stability and the performance of the system.

Measured response

As the clamping is far from being perfect on the real panel, the response of the actuator (figures 12e and 12f) has characteristics of both the theoretical response of an actuator bonded on a perfectly clamped panel and the theoretical response of an actuator bonded on a simply supported panel.

The first drop in the amplitude is not as deep as the predicted drop in both cases. Nevertheless, it appears at a frequency (5 kHz), which is situated between the frequencies of the drops for the clamped panel and the simply supported panel. The prediction of the frequency of this first drop is relatively accurate, because it is the result of a complex interference phenomenon which mainly depends on the distance between the sensor and the base of the triangle (see previous section). A second drop can be seen at around 20 kHz, which is a frequency that corresponds to the predicted frequency.

The first resonance frequencies are the same as the resonance frequencies with the clamped panel, which is logical since the stiffening effect due to the clamping is really significant at low frequencies. Though, the amplitude of these modes is higher than expected, and closer to the amplitude of the modes with the simply supported panel. This is a positive aspect of the real response, because it means that the actuation is relatively strong at low frequencies, so that the system should be efficient in this frequency range.

A phenomenon occurs at around 1 kHz that was not predicted in the simulations: the modes at these frequencies seem to be squeezed, and a phase shift is created, which creates instabilities. This effect is different from the effect that creates the drops in the amplitude, because experiments have shown that it is independent on the position of the sensor, which is not the case with the drops. It seems to be linked to the position of the actuator on the panel, and thus does not depend on its characteristics.

Other effects appear at higher frequencies (beyond 10 kHz), that were not predicted by the simulations. As these effects appear at high frequencies, they are probably due to the non-homogeneities of the panel, and to the boundary conditions. The glue, which has been used to bond the piezoelectric actuators on the panel, may also have a big influence on the response at high frequencies. As it is impossible to obtain a perfectly homogeneous layer the actuator's strains can have a different effect on the panel. Because the thickness of the glue layer is relatively small, these effects may only appear at high frequencies. A second effect of the actuators that can occur at high frequencies is the local mass and stiffening effect of the piezoelectric patch. Because they are localised, these effects are difficult to take into account precisely.

The measured response is interesting because the amplitude is very high at frequencies around 7 kHz, which corresponds to a frequency range where the system is stable (green loops on the Nyquist plot). As a consequence, the active control is not only efficient in the low frequency range as expected, but also at high frequencies, which is very good for the global efficiency of the system. Big loops appear on the left hand side of the Nyquist plot above 10 kHz, which could lead to instabilities and deteriorate the performance of the system. However, because accelerometers add mass effect, these loops are reduced in reality (see part 2.4.2).

In the following parts, the theoretical studies have been made with the simply supported panel.

2.3. Parametrical study

In order to design an optimal actuator, a parametrical study has been made to evaluate the influence of the height, of the base length and of the size of the actuator on the performance and the stability of the control system.

The criterion that has been used to evaluate both the performance and the stability of the system is the ratio between the maximum size of the right hand side loops and the maximum size of the left hand side loops of the Nyquist plot ($\delta = \frac{\delta_1}{\delta_2}$, see figure 14). This criterion is based on the following observation: as explained in part 2.2, the performance of the system at low frequencies is related to high amplitude of the response in this frequency

range, eg to big loops on the right hand side of the Nyquist plot. On the contrary, stability is given by relatively small loops on the left hand side of the Nyquist plot. As a consequence, the criterion using the ratio between these two values is able to assess both performance and stability: a high ratio means good performance and stability, and a low ratio means bad performance and stability.

Obviously, the δ ratio is not able to differentiate a very efficient system from a very stable system, but it allows evaluating the general assets of a system.

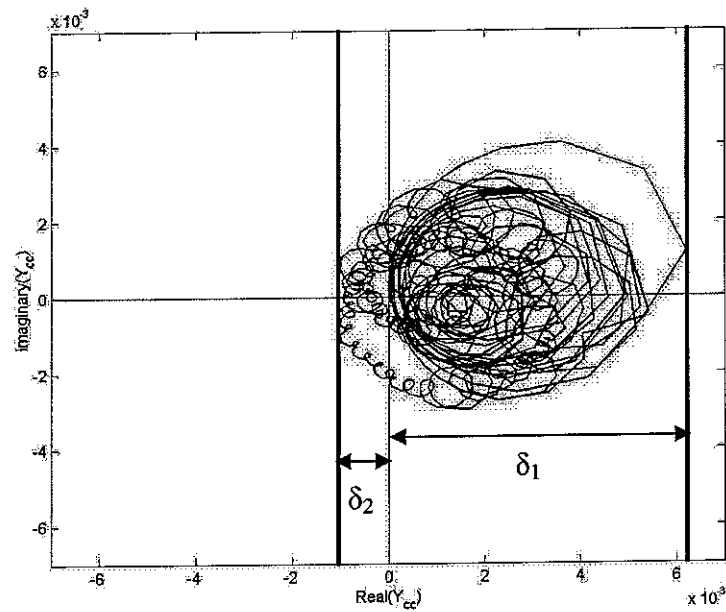


Figure 14: parameters used to assess performance and stability of a system

2.3.1. Influence of the actuator's height

According to the analysis that has been made in part 2.2, the height of the triangles is one of the most influent parameters for the performance of the system. In this section, the base length is equal to 40 mm. The δ criterion has been plotted as a function of the height of the triangles in order to evaluate the effect of this parameter on the performance (figure 15). The performance seems to increase with the height of the triangle. However, for very high values, the performance goes down. An optimal range for the height of the triangles can be found, which is in this case situated between 25 and 40 mm.

The different peaks that can be observed on this plot are due to the peaks (modes) in the frequency response function of the actuator. Changing the height completely changes the

dynamics properties of the actuator, which strongly modifies the Nyquist plot and the δ ratio. As a consequence, big differences appear between two different configurations, which produce the peaks in figure 15.

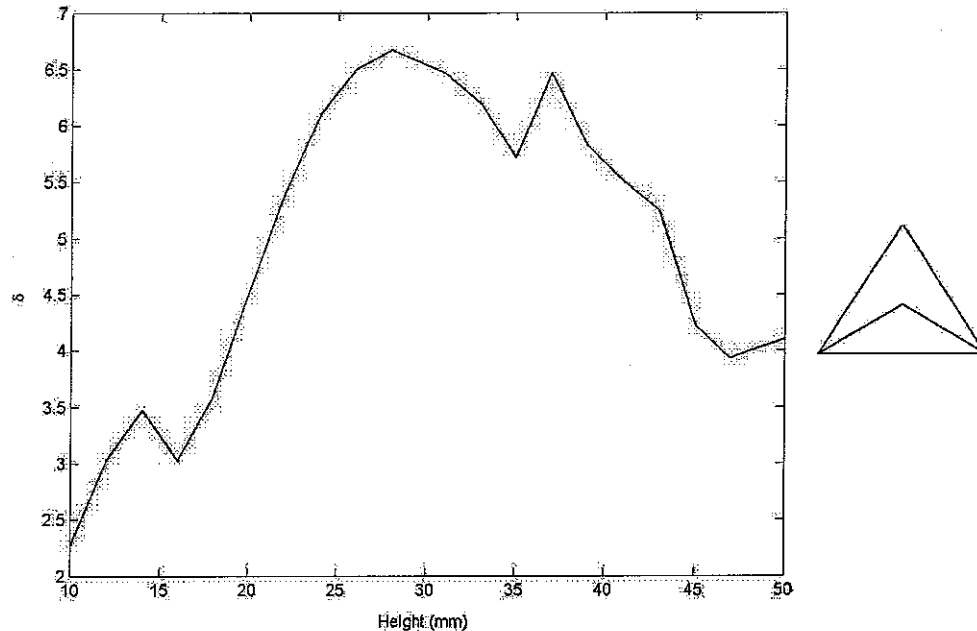


Figure 15: variation of the δ ratio with the height of the actuator

In order to explain more precisely the bad performance of the system for small and high values of the actuator's height, the Bode diagrams and the Nyquist plots of the response have been plotted for the two following values: 10 and 47 mm. The response of the actuator with the optimal value of 27 mm for the height has also been plotted as a reference (figure 16). It appears that the main reason why the δ criterion is so bad for small and high values of the height is that the stability becomes really bad for those values.

For very small values of the height, the amplitude of the response keeps increasing (unlike the response with "standard" values) whereas the phase goes down; thus, the loops of the left hand side of the Nyquist plot are relatively big, which means that the system is likely to go unstable. In that case, the response due to the moments on the right and left edges is completely different from the response plotted in part 2.2, as seen on figure 17, and becomes closer to the response due to the moments on the base. This explains the particular shape of the global response.

For high values of the height, many drops appear at high frequencies that have relatively high amplitude. As some of these high amplitudes correspond to the phase domain

[90° , 270°], the system has bigger loops in the left hand side of the Nyquist plot, and can potentially go unstable.

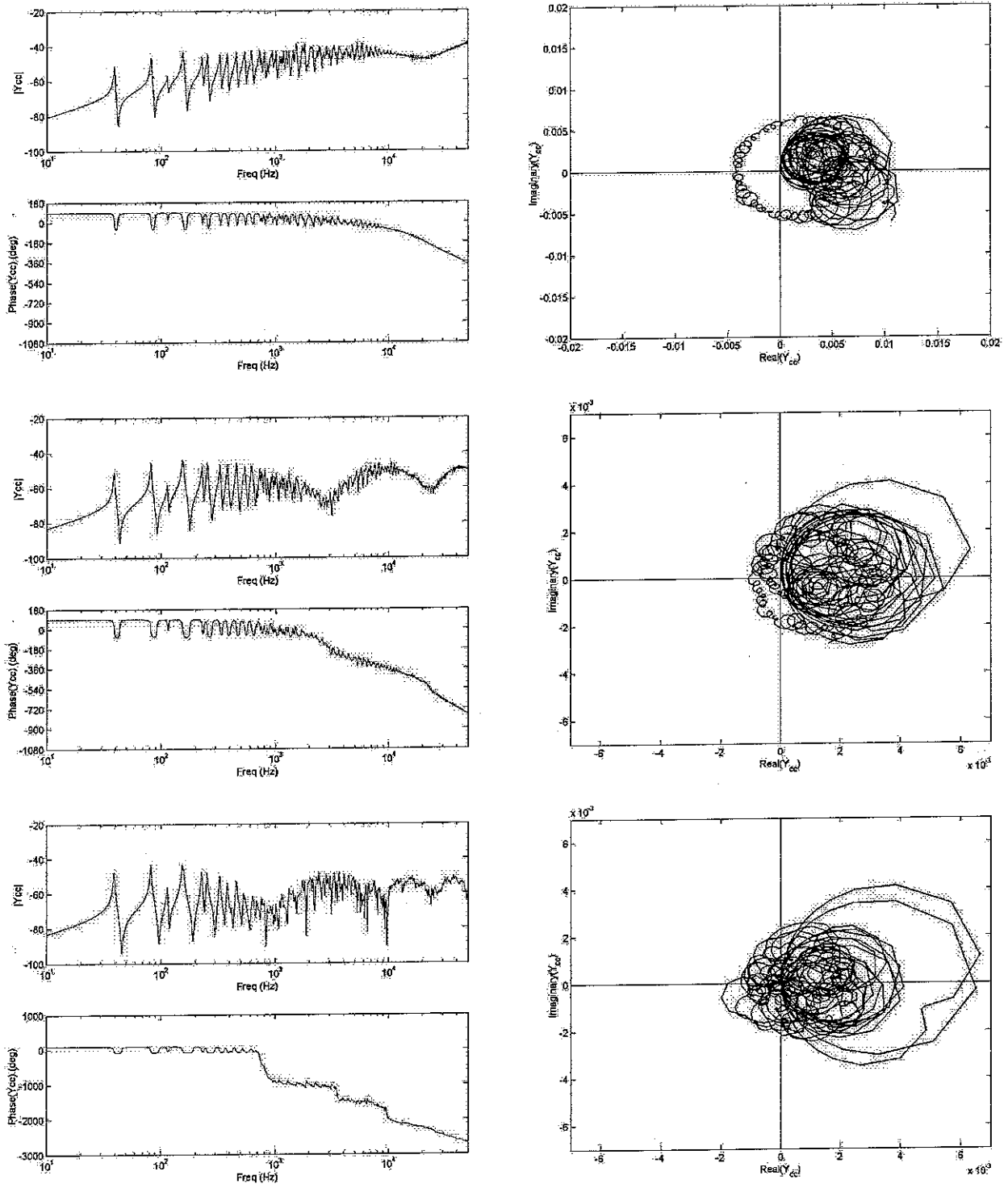


Figure 16: Bode diagrams and Nyquist plots with a height of 10 mm (1st row), 27 mm (2nd row) and 47 mm (3rd row) – simulated responses

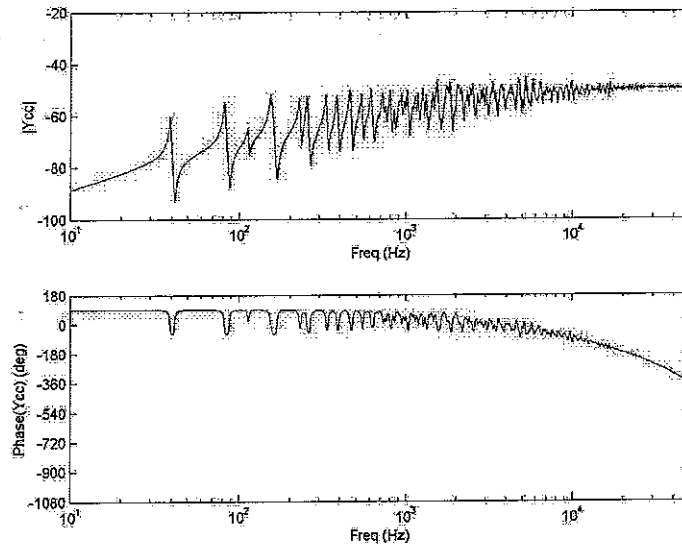


Figure 17: Bode diagram of the response due to only the moments on the left edge of the triangle with a height of 10 mm

The height of the triangle has also an influence on the frequency of the drops in the amplitude, since they are due to the distance between the points of application of the moments and the sensor's position, which creates a phase lag (see part 2.2). The frequencies of the three first drops have been plotted as a function of the height of the triangle (figure 18).

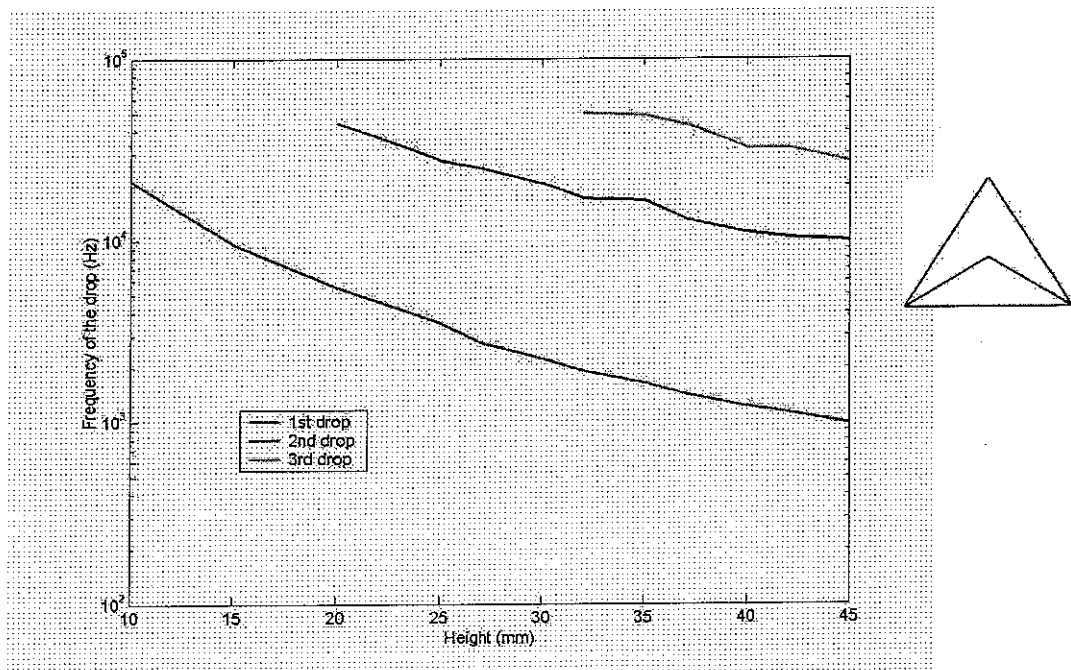


Figure 18: frequencies of the three first drops as a function of the height of the actuator

As expected, the frequencies of the drops in the amplitude of the response decrease when the height of the triangular actuator increases. The interferences (eg the drops) occur indeed at lower frequencies for higher values of the height.

Measurements have been made with a triangular actuator with the following dimensions: base: 40 mm and height: 10 mm. The corresponding Bode diagram and Nyquist plot are plotted in figure 19.

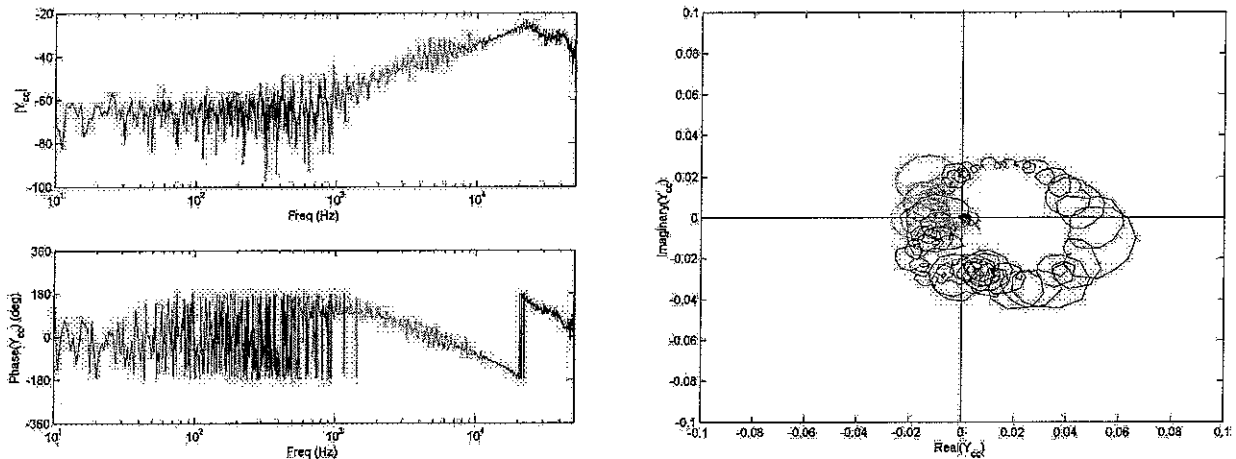


Figure 19: Bode diagram and Nyquist plot of the measured response with a height of 10 mm

As predicted in the simulation (figure 16, 1st row), the amplitude of the response of the actuator with a height of 10 mm goes up, and almost no drop can be seen below 10 kHz. This configuration is very bad for the stability because the size of the loops in the left hand side of the Nyquist plot is higher than the size of the loops corresponding to the low frequency modes, as predicted in the simulation. Thus, the system is likely to go unstable before being really efficient in this frequency range. The actuator is very efficient at very high frequencies, but this effect is cancelled when accelerometers are used (see part 2.4.2). The bad quality of the response is due to the fact that the sensor (laser) is placed close to the clamping, so that the signal is very weak.

The height of the triangular actuator is a very influent parameter for both the shape of the global response and the performance of the system.

2.3.2. Influence of the actuator's base length

In this part, the height of the actuators remains equal to 25 mm. The δ criterion has been plotted for different values of the base length. This plot shows that the performance and the stability of the system increase with the base length. Though, for high frequencies, the δ ratio goes down. The optimal value in this case is equal to 40 mm.

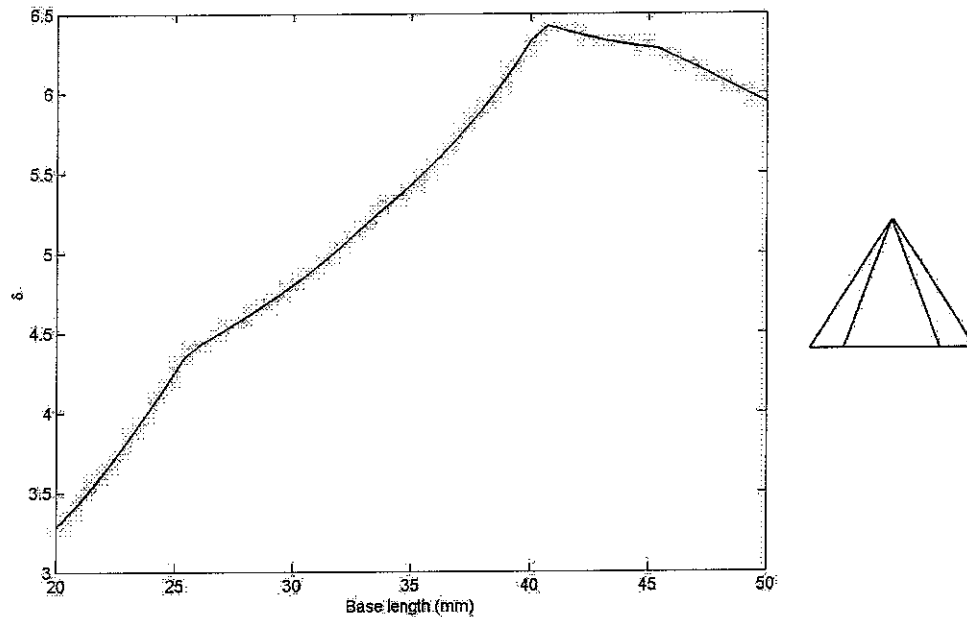


Figure 20: variation of the δ ratio with the base length of the actuator

The bad performance of the triangular actuator with small bases is due to the relatively high amplitude of the response at high frequencies, which leads to instability. It is the same phenomenon as with high values of the height, as described in the previous section (figure 16, 47 mm): the amplitude of the response at frequencies where instability phenomena occur is relatively high, so that the size of the left hand side loops in the Nyquist plot increases.

The response of the system with a very small base (20 mm) has been plotted in figure 21 in order to explain this effect for small bases. The Bode diagram of the response with a base equal to 20 mm clearly shows the influence of the moments on the right and left edges of the actuator on the second drop. The global response is indeed similar to the response due to these moments at high frequencies. In particular, the same drops can be seen beyond 30 kHz (see part 2.2).

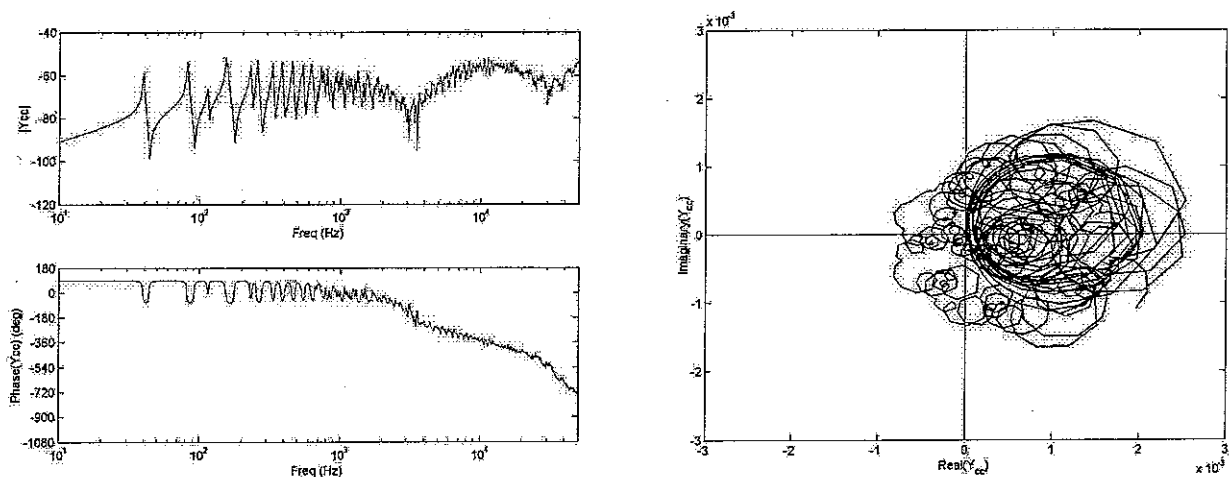


Figure 21: Bode diagram and Nyquist plot of the simulated response with a base of 20 mm

As for the height, the frequencies of the first drops in the amplitude of the response have been plotted as a function of the base length.

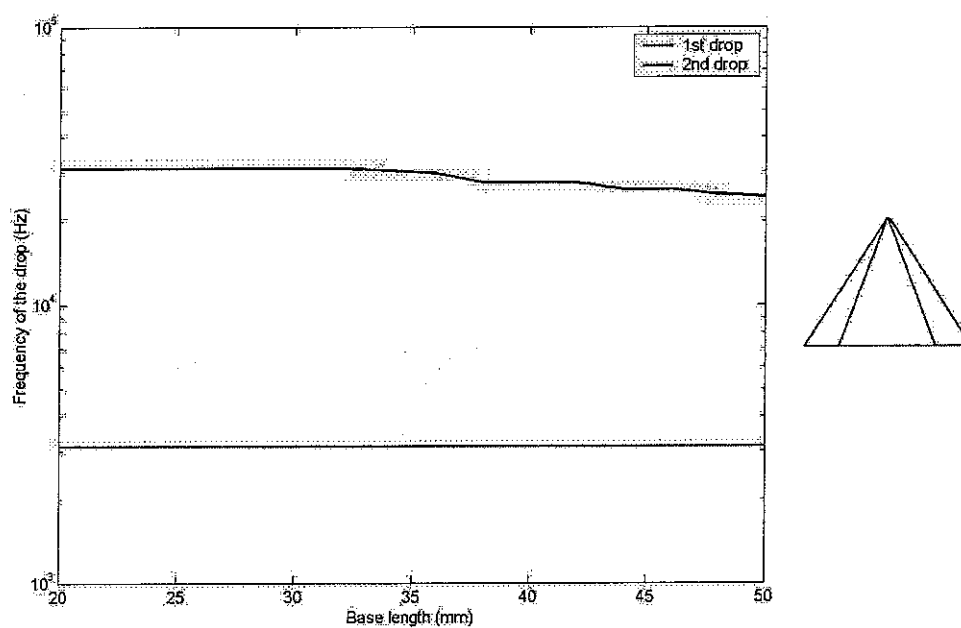


Figure 22: frequencies of the first drops as a function of the base length of the actuator

As expected, the frequency of the first drop does not depend on the base length, since it is directly linked to the height of the triangle. On the contrary, the second drop is also influenced by the moments on the right and left edges. As explained in part 2.2, the response

due to these moments is characterised by drops at high frequencies that contribute in the creation of the drops in the amplitude of the global response at high frequencies. As the contribution of these moments is modified when the length of the base is changed, the drops at high frequencies are also slightly modified.

The length of the base does not have a big influence on the shape of the global response of the actuator. Though, it plays an important role on the stability of the system, so that it has to be considered as an important parameter to design an optimal actuator.

2.3.3. Influence of the size of the actuator

In this part, the top angle's value remains constant, and both the height and the base are multiplied by a factor, so that the overall size of the actuator is modified. The δ criterion has been plotted as a function of the multiplication factor used to increase the size of the triangular actuator.

The δ criterion increases with the size of the actuator. When the size is increased, both the height and the base length of the actuator are modified, so that the variation is in that case a combination of the effect of the modification those two parameters.

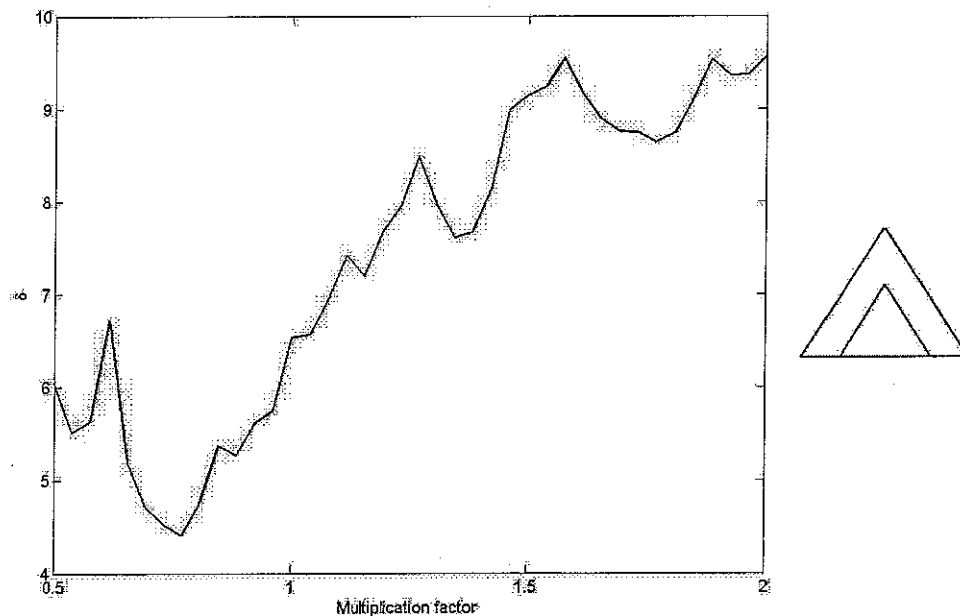


Figure 23: variation of the δ ratio with the size of the actuator

The actuation is much more efficient with bigger actuators. However, their size is limited by several constraints, and it is often impossible to use too big actuators. That is the reason why it seems more relevant to use the height and the length of the base as design parameters, instead of the size.

The frequencies of the first drops in the amplitude have also been plotted as a function of the multiplication factor (figure 24). This plot clearly shows a similar behaviour as for the height, which is logical, since the height has a big effect on the drops.

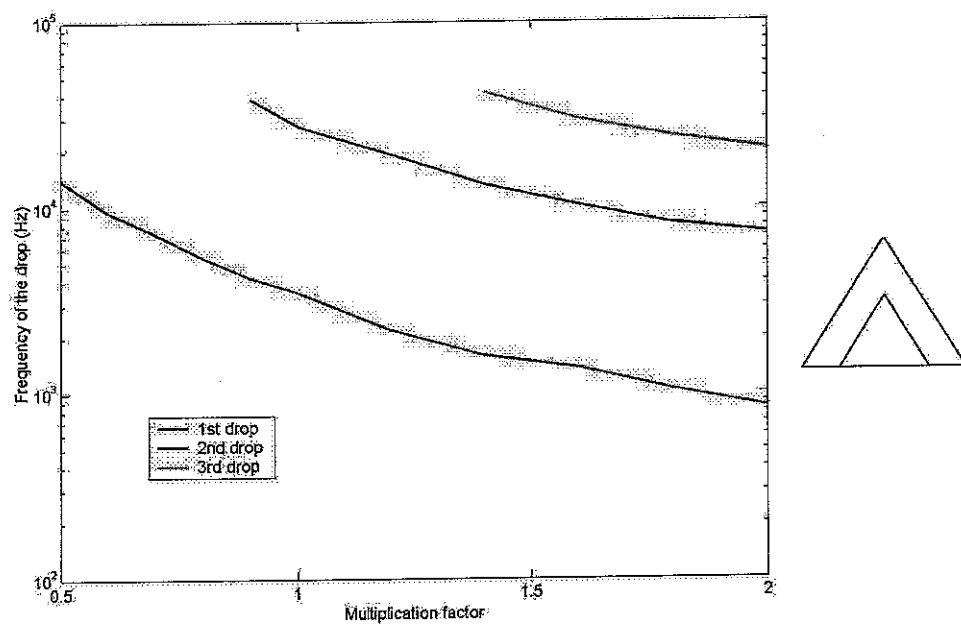


Figure 24: frequencies of the three first drops as a function of the size of the actuator

2.3.4. Optimal set of parameters

The δ criterion has been plotted as a function of both the height and the base length of the triangular actuator. As the influence of the size of the actuator is a consequence of the influence of these two parameters, it has not been considered in this part.

The highest values for the δ ratio are plotted in red in figure 25. This figure allows determining an optimal set of values for the base length and the height, which are situated between 40 and 50 mm for the base length, and between 25 and 40 mm for the height. For very small values of the height, it is necessary to have a smaller base in order to get an

efficient system, since triangles with sharp angles are more efficient than those with large angles.

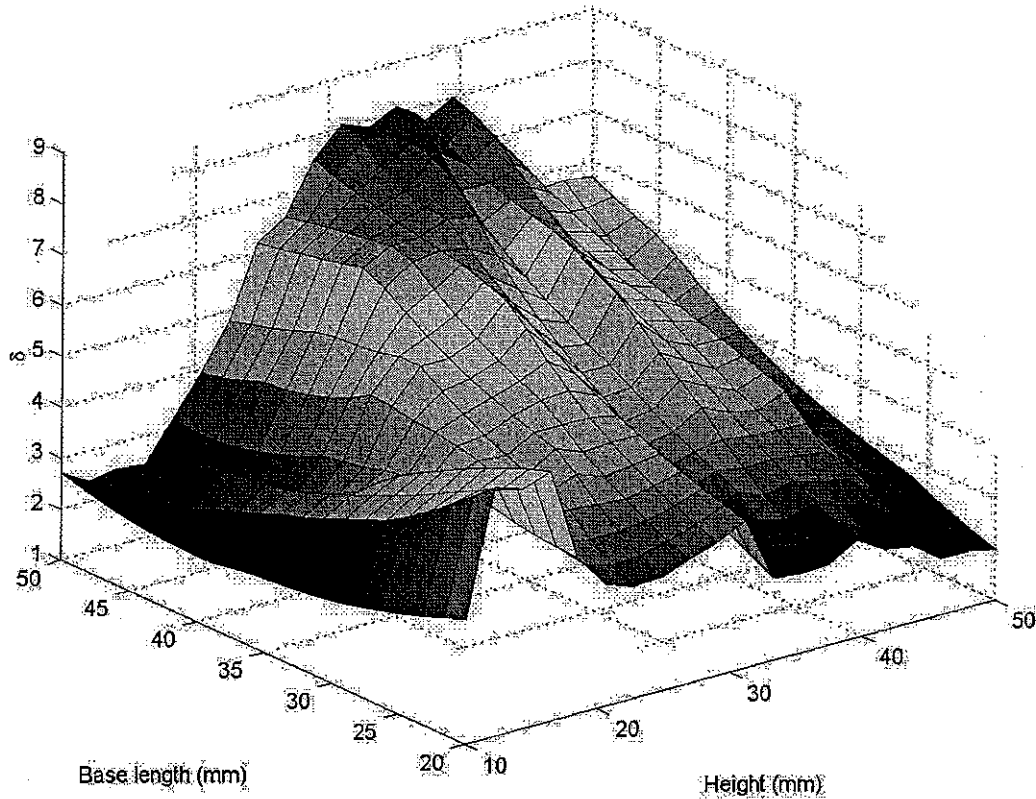


Figure 25: variation of δ with the height and the base length of the triangular actuators

It is very difficult to evaluate the performance of the actuator in itself, since its response is fully coupled to the system it is bonded on. That's why it is necessary to study the performance and the stability in each single case in order to get the best set of parameters adapted to one particular system. However, the general conclusion of this parametrical study is that actuators with sharp angles are more stable and efficient than actuators with large angles.

The performance of the actuator has been assessed assuming that the sensors where ideal velocity sensors. In the following part, the influence of the accelerometer has been integrated in the model.

2.4. Influence of the accelerometers

Even though the accelerometer doesn't seem to have a big influence on the measured response in the frequency range [10 Hz, 50000 Hz], it is interesting to see the effect that it should have in theory on the performance and the stability of the system.

2.4.1. Analytical model with accelerometer

A classical accelerometer can be seen as a single degree of freedom system made of a seismic mass connected to the vibrating system via a spring and a damper. In fact, the spring is a piezoelectric actuator that produces a signal proportional to the relative displacement between the mass and the base $w_{c2} - w_{c1}$ (see figure 27). This displacement is related to the acceleration of the base according to the following equation [3]:

$$H(j\omega) = \frac{w_{c2} - w_{c1}}{\ddot{w}_{c1}}(\omega) = \frac{-m_a}{(k_a - \omega^2 m_a) + j\omega \cdot c_a} \quad (21)$$

The Bode diagram of H has been plotted in figure 26. As any single degree of freedom system, the accelerometer has a resonance frequency. The figure 26 shows the example of an accelerometer whose resonance frequency is equal to 9000 Hz. A peak and a phase shift of -180° can be seen at this frequency.

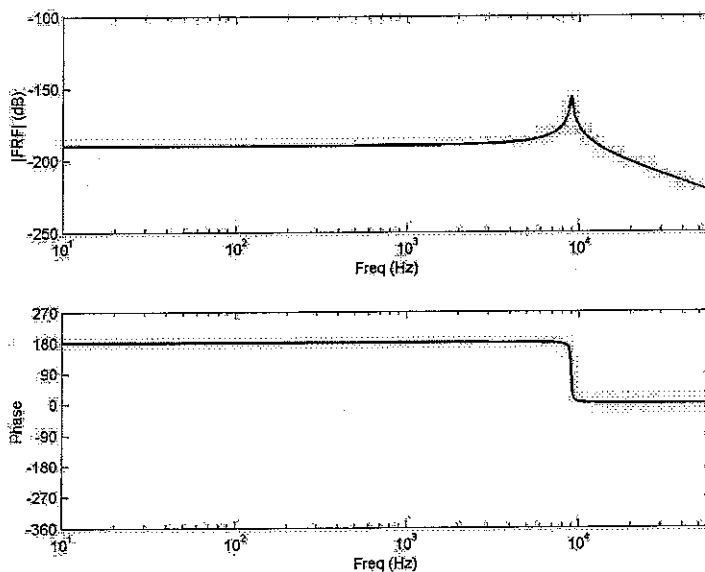


Figure 26: Bode diagram of the frequency response function of an accelerometer

In order to include the effect of the accelerometer in the analytical model, it is necessary to calculate both the velocity of the plate at the position of the accelerometer and the velocity of the seismic mass [3], which are shown on figure 26.

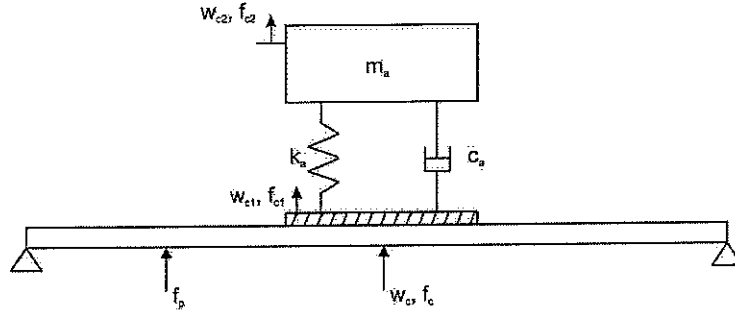


Figure 27: scheme of an accelerometer mounted on the panel

The velocity of the plate at the top of the triangle and the velocity of the suspended mass of the accelerometer can be expressed using the mobility formulation:

$$\begin{cases} \dot{w}_{c1} = Y_{11} \cdot f_{c1} + Y_{cp} \cdot f_p + Y_{cc} \cdot v_c \\ \dot{w}_{c2} = Y_{22} \cdot f_{c2} \end{cases} \quad (22)$$

Y_{22} is the mobility of the mass of the accelerometer, given by (Newton's law):

$$Y_{22} = \frac{\dot{w}_{c2}}{f_{c2}} = \frac{1}{j\omega \cdot m_a} \quad (23)$$

Equations in the system (20) can be grouped in matrix form as follow:

$$\dot{\mathbf{w}} = \mathbf{Y} \cdot \mathbf{f} + \mathbf{Y}_p \cdot f_p + \mathbf{Y}_c \cdot v_c \quad (24)$$

where:

$$\dot{\mathbf{w}} = \begin{Bmatrix} \dot{w}_{c1} \\ \dot{w}_{c2} \end{Bmatrix}, \quad \mathbf{Y} = \begin{bmatrix} Y_{11} & 0 \\ 0 & Y_{22} \end{bmatrix}, \quad \mathbf{f} = \begin{Bmatrix} f_{c1} \\ f_{c2} \end{Bmatrix}, \quad \mathbf{Y}_p = \begin{bmatrix} Y_{cp} \\ 0 \end{bmatrix}, \quad \mathbf{Y}_c = \begin{bmatrix} Y_{cc} \\ 0 \end{bmatrix}$$

By considering the dynamical behaviour of the accelerometer and the boundary conditions, \mathbf{f} can be expressed as following:

$$\mathbf{f} = -\mathbf{Z} \cdot \dot{\mathbf{w}} \quad (25)$$

where:

$$\mathbf{Z} = \begin{bmatrix} Z_{11}^a & Z_{12}^a \\ Z_{21}^a & Z_{22}^a \end{bmatrix} \quad (26)$$

$$Z_{11}^a = Z_{22}^a = \frac{k_a}{j\omega} + c_a \quad (27)$$

$$Z_{12}^a = Z_{21}^a = -\frac{k_a}{j\omega} - c_a \quad (28)$$

The mass effect of the case of the accelerometer can also be taken into account in equation (24) by adding the following term at position (1, 1) in the matrix:

$$Z_{case} = j\omega \cdot m_{case} \quad (29)$$

Thus, using equations (22) and (23):

$$\dot{\mathbf{w}} = (\mathbf{I} + \mathbf{YZ})^{-1} \{ \mathbf{Y}_p \cdot \mathbf{f}_p + \mathbf{Y}_c \cdot \mathbf{v}_c \} \quad (30)$$

The output signal of the accelerometer is given by:

$$v_a = c_\sigma \mathbf{d}_c \cdot (\mathbf{w}_{c2} - \mathbf{w}_{c1}) \quad (31)$$

so that

$$v_a = c_\sigma \mathbf{d}_c \mathbf{w} \quad (32)$$

where:
$$\mathbf{d}_c = [-1 \ 1] \quad (33)$$

and c_σ is the gain of the accelerometer

In order to obtain a velocity feedback, it is necessary to integrate this signal:

$$v_a = \frac{c_\sigma}{j\omega} \mathbf{d}_c \mathbf{w} \quad (34)$$

Using $\mathbf{w} = \frac{\dot{\mathbf{w}}}{j\omega}$, the input signal is given by:

$$\hat{v}_a = \frac{c_\sigma}{j\omega} \mathbf{d}_c \left\{ \frac{1}{j\omega} (\mathbf{I} + \mathbf{YZ})^{-1} \cdot \mathbf{Y}_c \cdot v_c \right\} \quad (35)$$

Finally, the transfer function with an ideal integrator is given by:

$$G(\omega) = \frac{\hat{v}_a}{v_c} = -\frac{c_\sigma}{\omega^2} \mathbf{d}_c (\mathbf{I} + \mathbf{YZ})^{-1} \cdot \mathbf{Y}_c \quad (36)$$

2.4.2. Effect on the frequency response function

In figure 28, the mass of the accelerometer has been taken equal to 1e-3 kg and the stiffness has been taken equal to 3.19e-6 N/m, so that the resonance frequency is equal to 9000 Hz. The damping ratio is in this case equal to 1%. The resonance peak appears very clearly in the amplitude of the response. As this resonance also produces a phase lag, it makes the system much more unstable than with an ideal velocity sensor. Indeed, a big loop appears in the left hand side of the Nyquist plot.

The accelerometers also produce a mass effect that strongly reduces the response of the system at high frequencies. This effect is really interesting since instabilities precisely occur at high frequencies, as it has been shown in part 2.2.

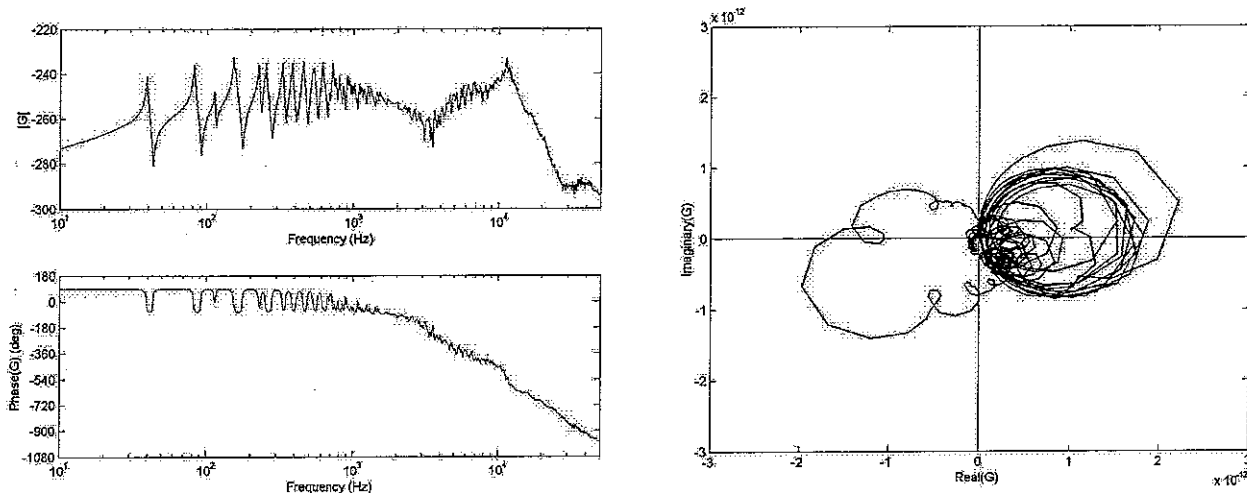


Figure 28: Bode diagram and Nyquist plot of the response with an accelerometer

By looking at the amplitude of the response of the feedback loop, it appears that if the accelerometer has a resonance frequency that perfectly corresponds to the frequency of the drop in the amplitude, the negative effect of the accelerometer can be cancelled. In order to assess this property, the δ criterion has also been plotted as a function of the resonance frequency of the accelerometer. In this plot, the seismic mass of the accelerometer remains constant and only the stiffness is modified.

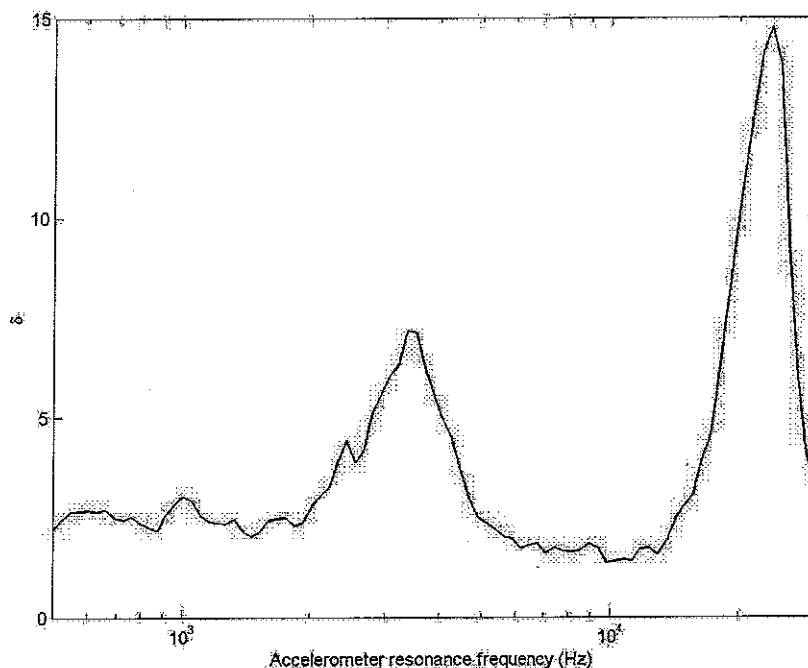


Figure 29: variation of the δ criterion with the resonance frequency of the accelerometer

Peaks appear at two frequencies, which means that the performance of the system is quite high. These frequencies correspond exactly to the frequencies of the two first drops in the amplitude of the response of the actuator (see figure 12a). This means that the system is much more stable if the resonance frequency of the accelerometer is designed to be equal to the frequency of one of the drops in the amplitude (or the contrary). As the resonance frequencies of the accelerometers are usually very high, it is obvious that this resonance frequency should match the frequency of “high order” drops, rather than the frequency of the first drop, whose frequency is relatively low.

The real accelerometers that have been used to carry out the experiments have a resonance frequency equal to 50 kHz, so that their effect is significant at very high frequencies. As this resonance is combined with the mass effect of the accelerometer, its influence is reduced. However, it is necessary to analyse the stability characteristics of the system over a very large frequency range even for applications at relatively low frequencies. The predicted and the measured response of the actuator bonded on the simply supported panel have been plotted in figure 30. The phase on the Bode diagram of the measured response has only been plotted from 200 Hz because of the bad quality of the response below this frequency.

The mass effect of the accelerometer can be clearly seen on the two responses. This mass effect allows reducing the size of the loops on the left hand side of the Nyquist plot, which improves the stability of the system. The differences between the simulated response and the measured response are due again to the stiffening effect of the clamping; in particular, the amplitude at low frequencies is much bigger with the simulations. Thus, the real system is more efficient between 5 kHz and 10 kHz because the amplitude of the response is high and the system is stable in this frequency range.

The loops on the left hand side of the Nyquist plot correspond to frequencies around the drops in the amplitude. In the measured response, the first instabilities are created by the “squeezing effect”, which occurs at around 1 kHz.

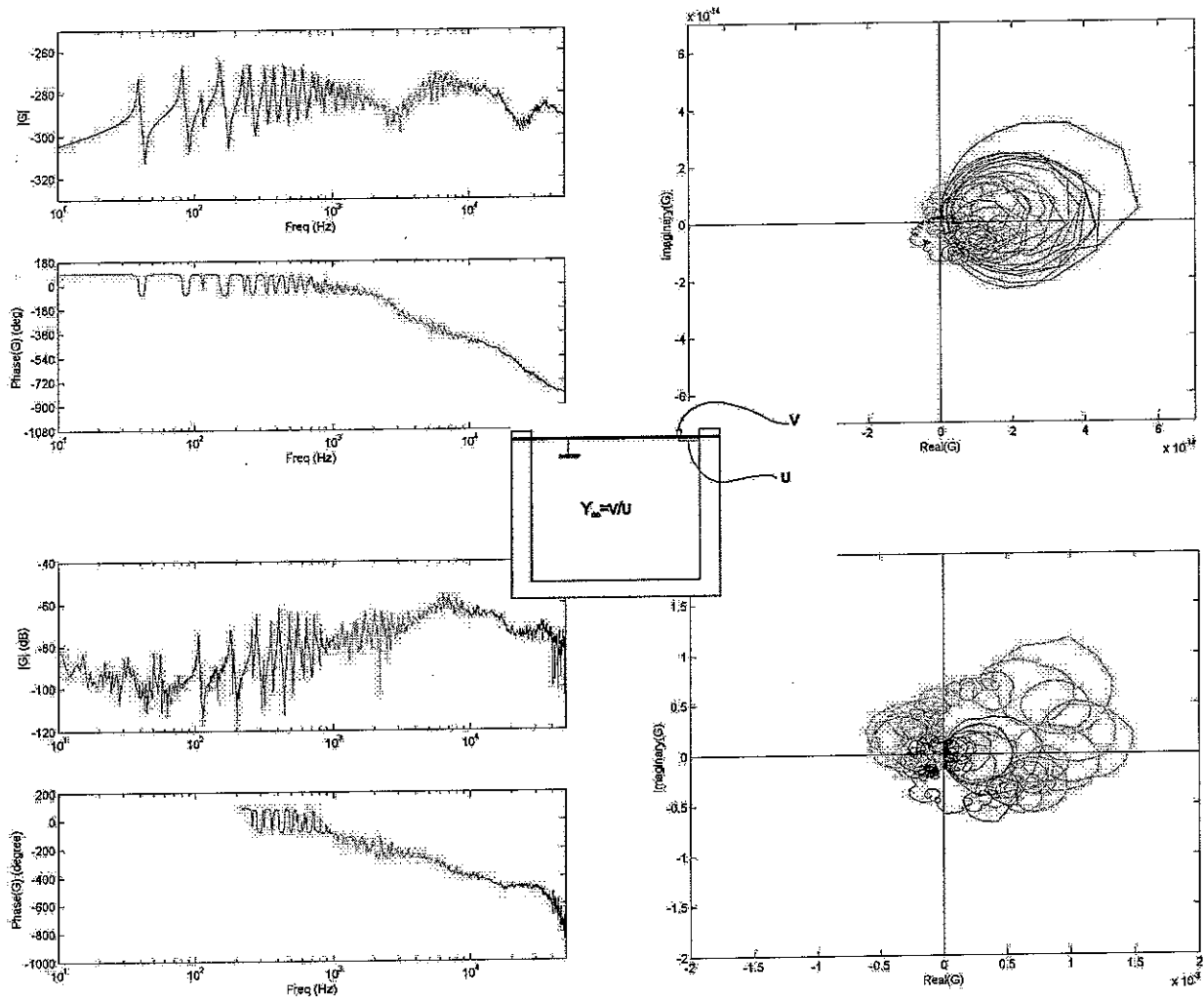


Figure 30: Bode diagrams and Nyquist plots of the simulated and measured responses with accelerometer

2.4.3. Influence of the position of the accelerometers

As it has been explained in part 2.2, the non-collocation between the sensor and the actuation is one of the main reasons why the system can go unstable, because it causes interferences between the different effects. However, it is interesting to analyse precisely the effect of the position of the accelerometer on the stability. Measurements have been made according to the scheme on figure 31, with the reference triangles (base: 40 mm, height: 25 mm).

As explained in part 2.2, the frequency of the first drop in the amplitude is lower if the accelerometer is placed far from the base edge of the triangle, because the phase lag is in that case more important.

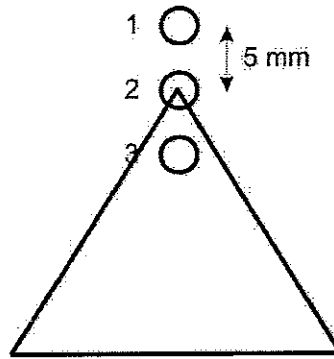
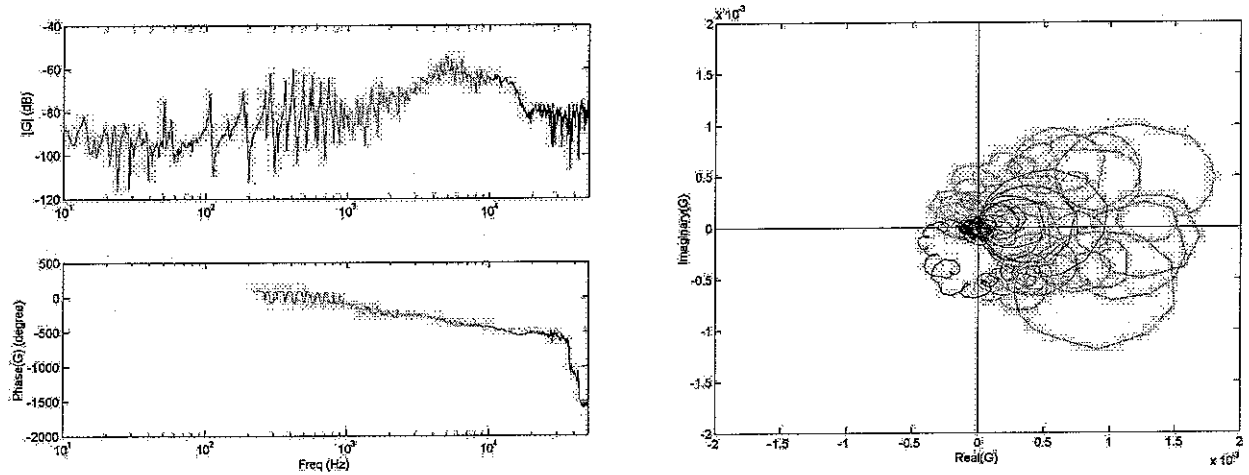


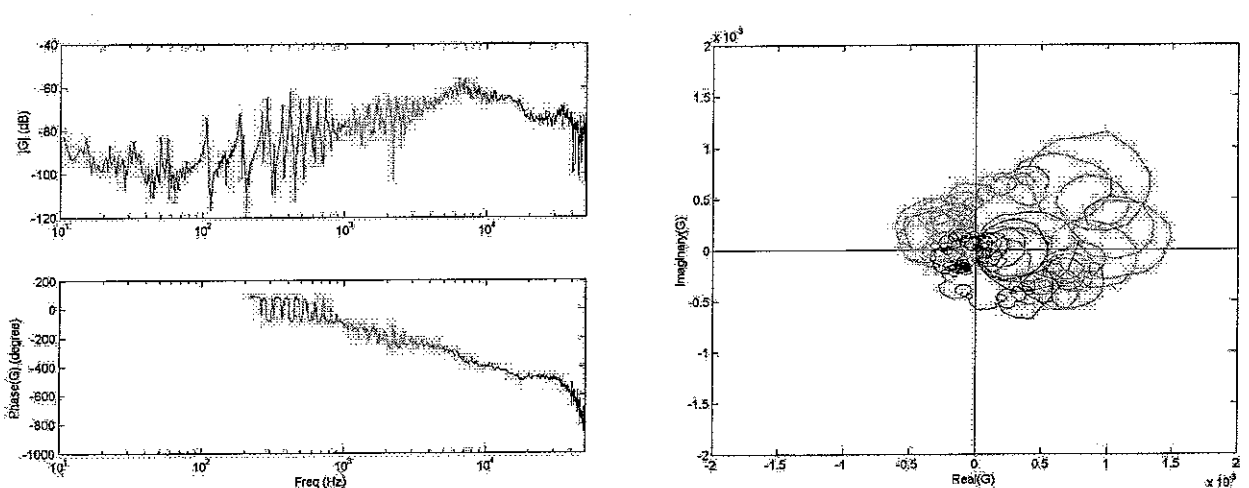
Figure 31: scheme showing the different positions of the accelerometer

This effect can be observed in figure 32. The drop even almost disappears when the accelerometer is too close to the base edge (position 3). The performance of the system is very bad in this case because the amplitude at frequencies associated to instabilities is relatively high.

Position 1



Position 2



Position 3

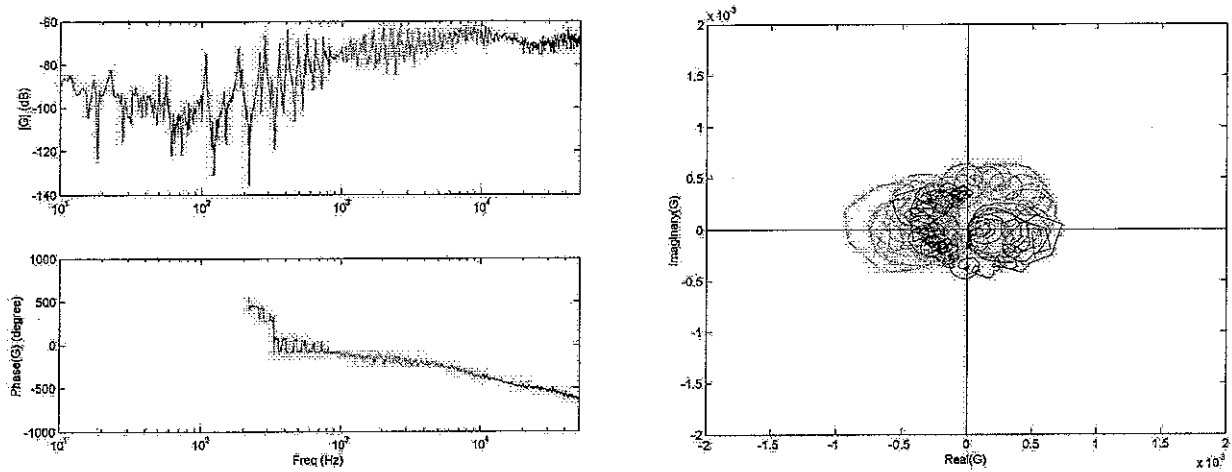


Figure 32: measured responses at the 3 positions (left: Bode, right: Nyquist)

These plots show that the global performance of a single unit is better if the accelerometer is placed outside the triangle, since the size of the left hand side loops of the Nyquist plot is smaller in that case. On the contrary, positioning the accelerometer inside the triangle leads to bigger loops on the left hand side of the Nyquist plot. In this case, a large part of the response is situated in the left hand side of the Nyquist plot, which means that the system is likely to go unstable over a relatively large frequency range.

The response of the system when the accelerometer is at position 1 is interesting because there is a combination between the drop in the amplitude and the “squeezing effect” described in section 2.2. Thus, the amplitude of the response at the frequency of the drop is much smaller, which is good for the stability since the response at this frequency is situated in the instability domain (left hand side of the Nyquist plot).

Measurements have also been made at positions on the left and right of the actuator, and gave similar results as those described previously. It confirms the fact that the influent parameter is really the distance between the sensor and the base edge of the triangle.

The optimal position of the accelerometer is difficult to evaluate theoretically, because many effects are not taken into account in the analytical model. The conclusion that can be made with the model is that the accelerometers have to be placed outside the triangle, over its top vertice. When the sensors are placed inside the triangle, the performance and stability are

always very bad. Measurements are necessary to find the best position of the accelerometer for each control unit.

The optimal position for the reference actuator (base: 40 mm, height: 25 mm) that has been used for the closed loop measurements, is situated 5 mm from the top of the triangle.

3. CLOSED LOOP SYSTEM'S EFFICIENCY

In this part, the velocity at the control point has been measured with the closed loop system, in order to evaluate its efficiency.

3.1. Frequency response function of the whole feedback loop

The panel is excited by a shaker. The signal measured by the accelerometer is amplified and fed back into the system through the triangular actuator. The scheme of the closed loop system is given in figure 33.

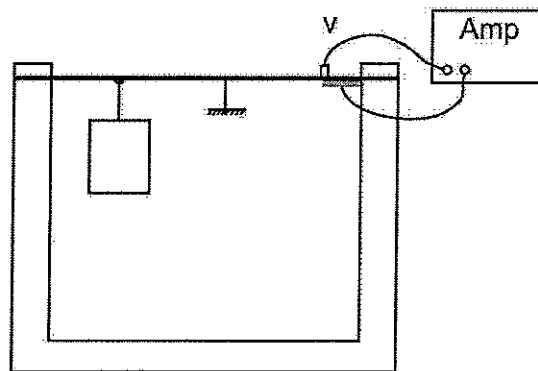


Figure 33: *scheme of the closed loop system*

The accelerometer is placed at the optimal position found in the previous section.

In order to achieve the best reduction of vibrations, the gain of the feedback loop has been optimized so as to obtain the biggest right hand side loops possible without reaching the instability point. The transfer function of the feedback loop with this optimized feedback gain has been plotted in figure 34.

As the amplifier that has been used to increase the gain of the feedback loop is not perfect, the shape of the Nyquist plot of the open loop is strongly modified. In fact, real amplifiers generally act like low pass filters, that introduce a phase lag of -90° at their cut off frequency. This phase lag changes the position of the different loops on the Nyquist plot. However, most of the loops remain in the right hand side of the Nyquist plot, so that the stability properties of the control system are not really modified in this case.

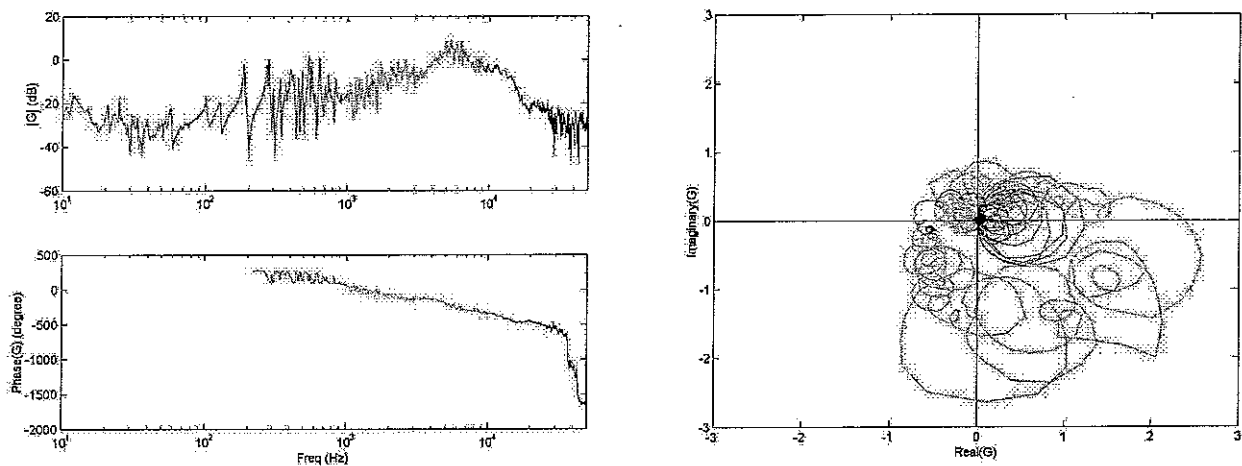


Figure 34: *frequency response function of the feedback loop with optimized feedback gain*

According to the Nyquist plot in figure 34, the system is supposed to be efficient in the frequency ranges corresponding to the right hand side loops. Thus, a reduction of the level of the vibrations is expected below a few kHz. The system is expected to have a bad efficiency around 10 kHz since the loops around this frequency are situated in the left hand side of the Nyquist plot.

As explained previously, these results are strongly dependant on the devices that are used to amplify the signal. That's why it is necessary to analyse the response of the open loop with all the amplifiers and filters (integrator...) in order to be sure to obtain the optimal feedback control. The optimal control system is a combination between the optimal actuator and the optimal feedback loop.

3.2. Response at the control point with velocity feedback control

The velocity at the control point has been measured and plotted in figure 35 with active control (red) and without active control (blue).

Below 1 kHz, the amplitude of vibrations at the control point is reduced of at least 5 dB ($20 \cdot \log|v|$) for almost all the modes. In most of cases, a reduction of 10 dB is achieved. Outstanding results are obtained between 3 kHz and 5 kHz: a reduction of the vibrations of 15 dB is achieved over almost all this frequency range. This is due to the high amplitude of the response at these frequencies.

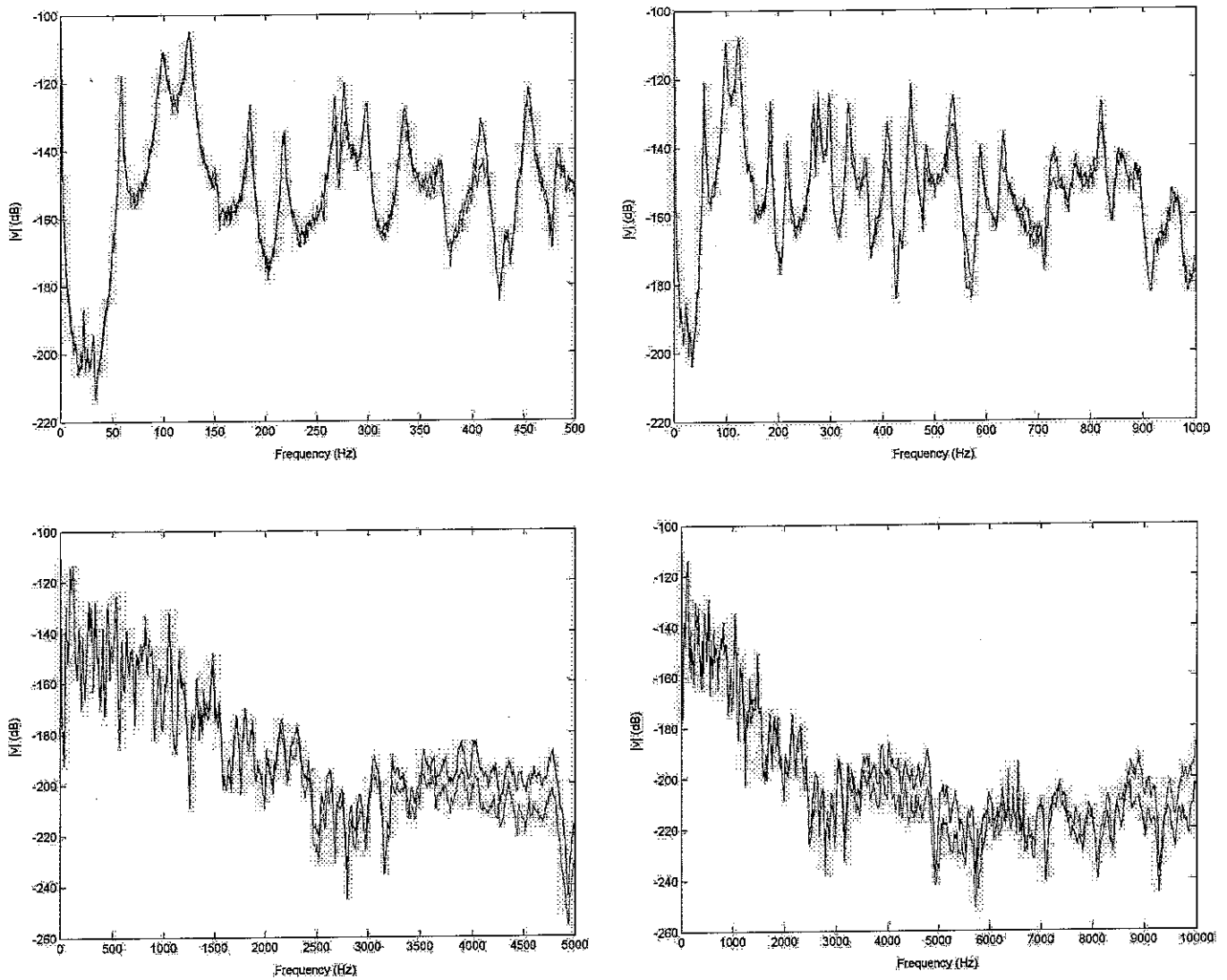


Figure 35: *measured velocity at the control point with active velocity feedback control for different frequency ranges. Results with one control unit*

The active damping effect can be clearly seen at low frequencies, where the amplitude of the resonances is strongly reduced, whereas the resonance frequencies are not modified. This damping effect could be even more efficient if higher gain could be used, which is impossible in that case because of instability phenomenon.

A deterioration of the response can be observed between 9 and 10 kHz. This is due to the left hand side loops of the Nyquist plot. As explained in part 2.1, the curve that is represented on the Nyquist plot is the response of the open loop. If this curve is situated on the left hand side of the Nyquist diagram, the real part of the open loop response is negative. At -180° , GH is less than 0, and thus $1+GH$ is less than 1. As a consequence the closed loop response function (given by equation 16) becomes higher than 1, which means that the

response is increased instead of being reduced. This is called the control spillover effect, and this is the reason why the vibrations level with active control is higher than the vibrations level without active control below 10 kHz.

These results are very interesting, since a reduction of the level of vibrations is not only obtained at very low frequencies, but also at frequencies up to 5 kHz. No spillover effect is observed in this frequency range, which means that the control system doesn't increase the vibrations level in this frequency range. Thus, the 16 decentralised units system should be able to achieve audible reduction of the transmitted sound. An improvement has still to be found for higher frequencies.

4. PERSPECTIVES

As explained in the previous sections, the triangular strain actuators are likely to amplify the vibrations of the panel at high frequencies, instead of reducing them. As this effect is directly due to the physical properties of the actuator, and cannot be avoided by changing its geometrical characteristics, another solution has to be found to improve the performance. As no spillover effect occur below 5 kHz, it seems relevant to use low pass filters with cut off frequencies situated below the first frequency where spillover effects occur. Such filters would strongly reduce the amplitude of the response corresponding to the spillover effect, and thus improve the performance of the system. Very good results have been achieved with square actuators, using an amplifier acting like a low pass filter. However, this amplifier could not be used for the triangular actuator because the static gain was not big enough to achieve good results.

Another way of reducing the spillover effect is to use phase compensators that are able to modify the Nyquist plot in such a way that all loops are situated in the right hand side of the Nyquist plot. In that case, very high gains can be used without reaching instability, so that the performance of the system can be very good.

However, using such devices makes the control system more complicated to use, and generally heavier. That's why miniaturisation is necessary to design optimal active control systems. Another issue for an industrial use is the power supply of the piezoelectric actuators that generally need high voltages to be efficient, which is often incompatible with the industrial constraints.

The main possible application of this kind of system is the active control of vibrations of a panel. It can be used as a solution to reduce the sound transmission of panels, where passive control treatments are not efficient. The position of the actuators along the borders of the panel is a real asset since it makes the design of the smart panel much easier, especially in terms of power supply, because cables can be mounted along the borders.

5. CONCLUSION

In this work it has been shown that the triangular piezoelectric actuators are well adapted to an active velocity feedback control of vibrations. This shape allows first a better collocation with the sensor, which is a key point for the stability and thus the performance of the system, since it produces a point force at its tip. It is also much more interesting than classical actuators because it can be designed precisely so as to obtain an optimal behaviour in a given situation. The main parameters have been studied and their influence on the stability has been assessed in order to obtain the optimal values for each of them. The performance of one single loop was measured, and gave promising results for the implementation of the sixteen units system.

Many improvements can be made, in particular concerning the signal processing of the feedback loop. As instabilities occur at high frequencies, which is a frequency range where the system is not supposed to be very efficient, it is possible to use low pass filters that cut the high frequency response. As a consequence, instabilities can almost be cancelled. First experiments have been made using this kind of filter, and gave very good results as well. The optimal control system will be a combination between optimal actuators and optimal signal processing.

More generally, this kind of active control system is really interesting since the feedback loop is really simple to implement. As each single actuator is driven independently, many filters and amplifiers have to be used. As a consequence, it is necessary to reduce their weight and size for an industrial use. However, other solutions can be used, such as centralised control systems, in which all the actuators are controlled by one single gain. This kind of system is less efficient, but it allows a considerable reduction of the number of filters and amplifiers that have to be used.

Further studies have to be carried out to improve the robustness of the system. Indeed, the actuator's response is strongly dependant on the system on which it is bonded, and on different external parameters. This can have very bad consequences on the stability of the system and thus of its integrity. This system could also be used to make active control in other frequency ranges: for instance, the velocity feedback control isn't generally very efficient in the mid frequency range, in which the transmitted power is not controlled by single modes but

by the mass of the vibrating system. In this range, the control system could be used in an acceleration feedback control, which allows an active mass control.

Although many improvements have to be made, active control using triangular piezoelectric actuators seems to have many interesting applications, both in the automotive and in the aeronautics industry, and thus constitute an interesting solution for noise reduction at frequencies where passive treatments are not efficient.

ACKNOWLEDGEMENTS

First of all, I would like to thank M. Paolo Gardonio who supervised my work at ISVR. I am thankful for the patience he had with me, and for the trust he gave me. Thanks to him I spent 5 very interesting months, both professionally and humanly, and I discovered a field I didn't know.

I am also grateful to the acoustics research department at Renault, and particularly to Ms. Virginie Maillard and M. Denis Ricot who supported this project and gave me the opportunity to do a very interesting work.

I would also like to address my thanks to all the ISVR staff, which has always helped me. In particular, Chinsuk Hong and Christoph Paulitsch spent much time help me do experiments I could not have done alone. I would like to thank M. Stephen J. Elliott for welcoming me in his team and Ms. Joyce Shotter for helping me when I needed.

REFERENCES

- [1] *Smart panel with multiple decentralized units for the control of sound transmission. Part 1: theoretical predictions, 2002.* P. Gardonio, E. Bianchi, S.J. Elliott.
- [2] *Smart panel with velocity feedback control systems using triangularly shaped strain actuators, 2004.* P. Gardonio, S. J. Elliott.
- [3] *Theoretical study of a velometer sensor – piezoelectric patch actuator pair for direct velocity feedback control systems, 2004.* M. Gavagni, P. Gardonio, S.J. Elliott.
- [4] *Modeling approach for two dimensional distributed transducers of arbitrary spatial distribution, 1996.* J. M. Sullivan.
- [5] *Advanced applications in Acoustics, Noise and Vibration, 2004,* F. Fahy, J. Walker.

ANNEXES

Physical properties of a simply supported panel:

- Natural resonance pulsation [5]:

$$\omega_n = \sqrt{\frac{D_p}{\rho_p h_p} \left[\left(\frac{m\pi}{l_{xp}} \right)^2 + \left(\frac{n\pi}{l_{yp}} \right)^2 \right]}$$

where

$$D_p = \frac{E_p h_p^3}{12 \cdot (1 - \nu_p^2)}$$

E_p is the Young's modulus of the plate, ν_p is the Poisson ratio, ρ_p is the density and h_p the thickness of the plate.

- Natural modes [5]:

$$\psi_n(x, y) = 2 \cdot \sin\left(\frac{m\pi x}{l_{xp}}\right) \sin\left(\frac{n\pi y}{l_{yp}}\right)$$

l_{xp} and l_{yp} are the dimension of the plate.

Radiation matrix:

$$\mathbf{R}(\omega) = \frac{\omega^2 \rho_0 A_e^2}{4\pi c_0} \begin{bmatrix} 1 & \sin_C(k_0 r_{12}) & \cdots & \sin_C(k_0 r_{1R}) \\ \sin_C(k_0 r_{21}) & 1 & & \vdots \\ \vdots & & \ddots & \vdots \\ \sin_C(k_0 r_{R1}) & \cdots & \cdots & 1 \end{bmatrix}$$

where $k_0 = \frac{\omega}{c_0}$ and r_{ij} : distance between the i -th and the j -th element

